Resilient Coastal Dune Ecosystems for Erosion and Habitat Protection at South Padre Island

Guna Eswar Kumar Uddagiri[1], Alayibo Semenitari[1], Oreoluwa Adeniyi Osiberu[1], Jashuva Melam[1], Jong-Won Choi[2], and Jianhong Ren[1]

[1]Department of Environmental Engineering, Texas A&M University-Kingsville

Kingsville, TX 78363

[2]Department of Civil and Architectural Engineering, Texas A&M University-Kingsville,

Kingsville, Texas

TABLE OF CONTENTS

PROJECT SUMMARY

Coastal dunes protect inland communities from sea-level rise, severe storm surges, flooding, and property damage. Planting of native vegetation is an effective method of strengthening coastal dunes along the coastline to increase dune stability. Vegetation has root systems that may entrap soil aggregates and consequentially, promote dune growth. Interactions of vegetation roots and soil particles result in (apparent) soil cohesion, which improves the apparent shear strength of sediment. However, there is limited data on the effect of coastline native vegetation on improving soil cohesion and reducing erodibility. Also, coastal dunes must maintain optimal geomorphological characteristics including height, width, and slope to successfully protect a coastal region from storm surges and floods. Dunes' morphology and volume are directly affected by forcing mechanisms such as tidal cycles, sea level change, sediment supply, wind, wave patterns, storms, hurricanes, human activities, and ecological factors such as the type and extent of vegetation. Elevation models of coastal dunes based on volumetric surveys such as using unmanned aerial vehicles (UAVs) may provide engineers and scientists with an efficient tool to evaluate their resiliency and stability against erosion from anthropogenic interventions and climate exposures. However, how effective and efficient these methods are in monitoring coastal topographical change in the South Texas coast remains unclear due to the specific site characteristics and environmental and weather patterns. In addition, the application of biodegradable coconut fiber in coastal dune restoration has been promoted as a nature-nurturing alternative along the US coast to combat coastal erosion and assist habitat restoration; however, quantitative data on the degradation rate of these fibers in

3

field conditions are very limited. Such information is critical in providing guidance during the design of coastal dune restoration efforts.

This project conducted various field data collections using a suite of techniques and extensive data analyses to tackle several data/knowledge gaps mentioned above. The work was conducted at the Isla Blanca Beach Park located in Cameron County, Texas where sand dunes have been restored along South Padre Island (SPI) since March 2019 with planting of vegetation recovered from demolished dunes. During the project period, data on vegetation density, root length density (RLD), % vegetation species coverage, NDVI (Normalized Difference Vegetation Index), apparent shear strength, and fiber mat degradation were collected and their temporal and spatial variations and correlations among relevant factors were evaluated. Wind speed and direction patterns were analyzed and the sediment transport rates were calculated. An analytical method was developed to quantify the dune morphological changes. The data obtained from the topographical surveys were evaluated to calculate the dune volume changes. A comprehensive analysis of survey methods with total station and UAV and their application in monitoring coastal dune restoration at SPI was conducted.

Results show that the vegetation densities are generally higher during the rainy season (March through September), which is consistent with the stronger correlation found between the precipitation and the vegetation density. Monocot species are more prevalent than the dicot species and they also exhibit a stronger correlation with precipitation than the overall vegetation density and RLD. NDVI is a promising indicator for long term continuous vegetation monitoring and can be explored more in future studies. The spatial variability of vegetation density and % monocot coverage is found to be significant and the RLD variability is significant with respect to time only. Sediment with vegetation exhibits greater shear strength than that without vegetation.

The results presented here suggest that the use of native vegetation, especially monocot species, with fibrous below-ground biomass (i.e., vegetation roots) can help strengthen restored dunes in coastal dune restoration projects, by increasing resistance to erosion and ultimately their resilience to climate challenges. Below-ground dynamics, represented by RLD, have a greater impact on sediment shear strength than the contribution by vegetation density, which is consistent with previous studies. A difference in dune growth rate from that calculated using Bagnold's model (2.91 m^3/m) to the one estimated based on the topographical survey data (3.97 m^3/m) was found and it can be attributed to factors not included in Bagnold's model, such as vegetation, temperature, precipitation and wave characteristics. The topographical survey and elevation model's results obtained from UAV offered valuable insights into the effectiveness, accuracy, and adaptability of the survey techniques, contributing to a deeper understanding of coastal dynamics.

Chapter 1. Introduction

U.S. coastal counties are currently experiencing unprecedented threats from climate challenges including intense rains, severe storms, high tide flooding, and sea level rise. Hurricane intensity has also increased over the past four decades (IPCC, 2021a, b). As the global temperature increases, more intense hurricanes and increased rainfall (IPCC, 2021a, b) are predicted. Meanwhile, sea level rise will create a profound shift in coastal flooding over the next 30 years by causing tide and storm surge heights to increase and reach further inland. Sea level rise is also accelerating coastal land erosion and ultimately land loss. Climate change along coastal communities affects not only human beings, but also properties, infrastructure, and services (EPA, 2023).

In response to the climate challenges, coastal sand dunes on barrier islands and coastlines are receiving great attention as a vital component of the coastal defense by absorbing wave energy while providing natural habitats for diverse flora and fauna (Durán Vinent et al., 2020). Damage assessment by Hurricane Sandy in 2012 demonstrated that communities protected by coastal dune systems suffered fewer damages than those without protection (City of New York, 2013; USACE, 2013; Walling et al., 2014), validating the benefit of dunes to coastal resilience. In recent years, therefore, coastal sand dunes have been constructed to mitigate climate change, enhancing the natural resiliency of coastal systems (Sigren et al., 2014). However, the dynamics of coastal morphology associated with sand dunes produced by the interaction of ecological and physical processes are not fully understood (Durán Vinent et al., 2021). Thus, the systematic application of sand dunes to coastal management plans based on scientific data is still limited.

1.1 Coastal Dunes, Vegetation, and Shear Strength

Coastal dunes are mounded with different layers which have been deposited in succession forming a structure of primary, secondary, and tertiary dunes depending on the location from the shoreline. That is, the nearest to the shoreline are the primary dunes, with secondary and tertiary dunes developing further inland (Jin et al., 2015). Dunes' morphology and volume are directly affected by forcing mechanisms such as tidal cycles, sea level change, sediment supply, wind, wave patterns, storms, hurricanes, human activities, and ecological factors such as the type and extent of vegetation (Griggs and Reguero, 2021). Coastal dunes become more susceptible to erosion as a result of a decrease in vegetation which is accelerated by increased human population and activities in coastal regions (Gallego-Fernández et al., 2011; Martínez et al., 2006). Various approaches have been adopted over the years to mitigate coastal erosion. Recent research has shown that regardless of wave intensity, beach-dune morphology, and erosion mode, vegetation plays a significant role in reducing dune erosion and recovering impaired or disrupted dunes (Gallego-Fernández et al., 2011; Houser and Mathew, 2011). The decline in dune erosion volume has been found directly correlated with both the in-situ shear strength of the dune and the density of the vegetation roots (Lancaster and Baas, 1998; Ajedegba et al., 2019). In addition, vegetation type also influences coastal dunes' resistance to shear with monocot vegetation being more suitable for dune restoration and providing stability compared to dicot native vegetation (Ajedegba et al., 2019).

Different methods have been used globally to strengthen the dunes and protect the coastal infrastructure which are vulnerable to natural and anthropogenic influences. For example, to protect the infrastructure and reduce costs, artificial dunes have been built towards the seaward side by moving the sand from local sources. Wooden walkovers are built over coastal dunes to

prevent tourists from trampling on them (Nordstorm and Jackson, 2022). Particularly, coastal dunes have been reinstated and maintained through intentional vegetation restoration. It is now well recognized that vegetation reinforces dune sediments with its root system providing extra resistance to erosion while its stem and leaves dissipate wave energy from storms to reduce erosion. Vegetation also helps trap wind-blown sediments, resulting in the volumetric growth of dunes (Feagin et al., 2015; Bryant et al., 2019). Roots of vegetation physically bind soil particles, which leads to increased shear strength of the sediment and ultimately enhanced resistance to erosion (Miller and Jastrow, 1990; Pollen, 2007; Veylon et al., 2015; Feagin et al., 2015). So far, most of the studies on the benefits of vegetation to the stability of sediments have focused on the interactions of vegetation roots and sediments on soil slopes (e.g., Waldron and Dakessian, 1981; Wu et al., 1988; Pollen and Simon, 2005). Field data on the quantification of the benefits of vegetation to dune stability is currently scarce (Feagin et al., 2015; Bryant et al., 2019). Particularly, field data on the contribution of dune vegetation (e.g., bitter panicum) with fibrous root system (Zhang et al., 2014) to the shear strength of sediment is still limited to the best of our knowledge (e.g., Wu and Watson, 1998; Fan and Su, 2008). Therefore, even though the role of vegetation in stabilizing coastal dunes along barrier islands and coastlines and their resilience to major storms has been phenomenologically described in the coastal management plans, the fundamental mechanism of the interactions between vegetation and dune sediment has not been fully explored (Sigren et al., 2014).

In addition, biodegradable coconut fiber mats, a biodegradable, ecofriendly and sustainable material being used around the world for erosion control projects, have recently become widely used in coastal dune restoration. Limited field observation data has indicated that these mats combined with monocot native vegetation species with dense fibrous roots

significantly reduced the erodibility of coastal dunes by 67 percent (Patel, 2020). To better

incorporate these mats in coastal dune restoration design, more quantitative data on critical

information such as the degradation rates of these materials in field conditions are required.

1.2 Monitoring Dunes' Morphology for Erosion Resilience Assessment

Coastal dunes play a crucial role in serving as a first line of defense against severe

weather conditions (Abbate et al., 2019; Bonte et al., 2006). Dunes protect coastal regions by

absorbing and dissipating the hydrodynamic energy produced by storm surges (Ciavola et al.,

2014). They also provide essential services such as sediment deposition, water catchment and

purification, habitat for wildlife, carbon sequestration, tourism, recreation, and education

(Ciavola et al., 2014). Coastal dunes must maintain optimal geomorphological characteristics

including height, width, and slope to successfully protect a coastal region from storm surges and

floods (Ajedegba et al., 2019; USACE, 1984), and thus it is of great importance to monitor such

characteristics for better management of coastal regions.

Elevation models of coastal dunes based on volumetric surveys may provide engineers

and scientists with an efficient tool to evaluate their resiliency and stability against erosion from

anthropogenic interventions and climate exposures (Zaghloul, 1992; Houser and Mathew, 2011).

To this end, various topographic surveying techniques (e.g., photogrammetry with aerial

photographs, total station, LiDAR, etc.) have been developed. Each method has its own level of

accuracy, efficiency, advantages, and disadvantages. Among these methods, the total station (TS)

has demonstrated accurate measurement of individual point coordinates. Its use in monitoring

changes in sand beach areas was recommended by Lee et al. (2013) based on the comparison of

its accuracy with RTK-GPS (Real-time kinematic Global Positioning System). However, in TS

surveying, if the coordinates are not georeferenced, it is difficult to transform the precise TS data

to an accurate global position without degrading the high relative accuracy and precision of the survey data (Khalil, 2013). The accuracy of the TS survey is also affected by factors including angle and distance of sight, weather conditions, etc. (Wyoming Department of Transportation, 2014).

Unmanned aerial vehicles (UAVs) demonstrate a wide range of applications in overseeing dynamic natural landscapes, such as monitoring changes in land formations and coastlines (Taddia et al., 2019; Zimmerman et al., 2020). UAVs are advantageous in mapping and surveying otherwise inaccessible areas, such as high-relief terrain or areas with dangerous vegetation and wildlife (e.g., cacti, snakes, etc.), while minimizing potential damage to the flora and fauna (Nesbit et al., 2022). The reliability and affordability of UAVs were confirmed by Taddia et al. (2019) through the Structure-from-Motion (SfM) approach while assessing the evolution of embryo dunes. The SfM technique involves a highly redundant, iterative bundle adjustment procedure, which uses a database of features extracted from multiple overlapping images to generate 3D structures (Snavely et al., 2008). Combining UAV surveys with the SfM technique presents an efficient, effective, dependable, and precise method (e.g., Zimmerman et al., 2020). However, the processes involved in the photogrammetric method are usually time-consuming and its accuracy can be reduced if not used properly (Barba et al., 2019).

1.3 Wind, Sand Transportation, and Sand Accumulation Model

Coastal dunes exist in a dynamic environment along the shore and are affected by sediment availability, prevailing conditions of winds and waves, precipitation, and beach characteristics. The waves transport sand from the foreshore (the area covered by normal daily tides) to the backshore (the area covered on the beach when there are storm tides and high spring tides) resulting in the growth of the beach (Del Angel, 2011). The sediment from the beach is

then transferred through an aeolian transport mechanism in the direction of the prevailing wind. Then the frontal part of the dune captures the travelling sand and holds it resulting in dune growth. The dune formation and sand accumulation depend on in-situ conditions such as sediment characteristics, dune topography, and vegetation cover (Del Angel, 2011).

Wind plays a vital role in sediment transportation along the beaches in coastal areas. When the wind blows over a surface covered with cohesionless sediment at a sufficient speed, the sand particles are subjected to lift and drag forces (Zaghloul, 1992). The sand particles enter the air stream when the resultant lift and drag forces exceed the weight and cohesive forces. Then the particles start moving horizontally in a trajectory in the wind direction. After a certain height is achieved, gravity tends to result in the descent of particles towards the land surface. The descending particles possess kinetic energy resulting in their rebound, causing the other particles to be dislodged into the air. This process is known as saltation (Zaghloul, 1992). The rebounding of the particles depends on the bed surface. For example, a rugged surface results in the vigorous bouncing of the particles with minimum energy dissipation (Zaghloul, 1992). In loose sand beds, the falling particles disturb the surrounding particles and bounce slightly or rest on the surface. The result of the continuous disturbance of the surface is a slow forward creep of the top layer of the bed surface; this mode of transportation is known as surface creep (Zaghloul, 1992). The mode of transport where the small grain-size particulates remain in the air for long periods is known as suspension (Zaghloul, 1992).

Wind and steady sediment supply are critical factors in dune formation or development. Dunes are formed when the wind-blown sand is trapped by vegetation or wrack on the beach. The quantity of sediment transported from the beach to the dune is related to the average wind speed and direction (Del Angel, 2011). The magnitude of sediment transport concerning wind

11

speed and direction can be calculated using different aeolian transport models. A good number of models have been developed for calculating the sediment transport rates over the past few decades including those proposed by Bagnold (1941), Hsu (1977), and Lettau and Lettau (1978). In aeolian transport models, sediment transport rate is often related to wind shear velocity or threshold shear velocity, which is based on the momentum transfer between moving sand particles and airstream (Dong et al., 2003).

Bagnold (1936) introduced a sediment transport model based on an elementary approach under certain conditions. Sediment transport models generally include various parameters due to the complexity involved in sediment interactions (Termini and Fichera, 2020). Most of the transport models utilize standard parameters such as grain size, wind shear velocity, air density and acceleration due to gravity (Sherman et al., 1998). The assumptions in aeolian transport models include uniform sediment size, steady and turbulent flow, unidirectional wind field, and dry sediment material. The factors that may influence the sand movement along beaches are precipitation, temperature, sediment and beach characteristics. Dune volume changes in coastal regions can be predicted based on sediment transport rates which are estimated utilizing the study area's wind data and sand transport equations. It should be noted that the results of the transport models often exceed the measured data due to limitations from the assumptions on which they are based (Arens, 1997).

Bagnold developed a sediment transport model after he conducted a series of wind tunnel experiments (Bagnold, 1936). Bagnold's model was the first experimental-based model and has been widely used since then. Bagnold relates sediment transportation by wind to the saltation process. Bagnold's equation suggests that the volume of sand transported is proportional to the third power of friction velocity (Bagnold, 1936).

1.4 Objectives of this Study

Padre Island is a barrier island along the coast of Texas, and it is the longest barrier island (182 km long) in the world. Padre Island is divided into North Padre Island and South Padre Island (SPI) by the Port Mansfield Channel (National Park Service, 2022). Padre Island has been protecting the coastline of Texas from waves and flooding from storms while it provides habitats for diverse native plant species and wildlife including diverse birds and the endangered Kemp's ridley sea turtles (Bessette et al., 2018). This unique situation of the island has attracted a series of research efforts including the investigation of vegetation and topography along its coastline (Judd et al., 1977; 1983; 2008; Lonard et al., 1999; Bessette et al., 2018); However, these studies focused on a phenomenological description of their correlation without quantitative evaluation of the contribution of various factors such as vegetation and wind to the stability of sediments.

The objectives of this study were to 1) collect sediment and vegetation data from newly restored sand dunes located at SPI, 2) suggest a method recently introduced to measure in-situ shear strength of vegetated sediments for cost-effective dune monitoring, 3) identify the contribution of vegetation to the stability of sand dunes based on in-depth analysis of collected field data, 4) develop protocols and methods to calculate the sediment transport rate and track the changes in the sand dune volume and topographical profiles, 5) quantify trends and patterns of sand dunes based on surveys with TS and UAV in mitigated areas of SPI, Cameron County, Texas, and 6) assess the degradation rate of fiber mats used to reinforce the restored dunes. In the following sections, methods, findings, and conclusions corresponding to each of the objectives are presented in sequence.

Chapter 2. Native Vegetation Assessment in South Padre Island Restored Areas

Currently, there is only a limited number of data sets available on the role of vegetation in enhancing sand dune stability (Wieder and Shoop, 2018); however, root tensile strength directly increases soil shear strength and augments the confining pressure of the soil (Fattet et al., 2010). Considering the impact of sand dunes on coastal communities, including protection against extreme events, support for local ecosystems, and economy (e.g., recreation, tourism, aesthetics, etc.) (Silva et al., 2016), it is of great importance to monitor the presence of vegetation and understand its reinforcement mechanism to improve dune stability. This chapter summarizes work conducted to assess vegetation distribution at the study site.

2.1 Study Area

The vegetation data collection was carried out at Isla Blanca Beach located at the southern tip of SPI (Figure 2.1), where several sand dunes were demolished and new sand dunes were built in 2018 by Cameron County, Texas. The dune restoration includes relocation of the removed sediments and replanting of the vegetation from the demolished dunes to newly restored ones. After replanting, to promote the growth of the vegetation, temporary irrigation systems were installed, and bio-degradable coconut fiber mats were placed at the toe of the new dunes and the fiber mats were completely degraded within a year.

Figure 2.1: Project location and mitigation areas of the restored sand dunes.

The Isla Blanca Beach Park restoration area was subdivided into four sub-areas (MA-2, MA-4, MA-5, and MA-6) (Figure 2.1). Among them, we collected data in two areas, MA-4 and MA-5 (Figures 2.1 and 2.2); both restored in August of 2020. No initial data collection was conducted immediately after the restoration since the COVID-19 pandemic led to limited access to the sites in 2020. Bitter panicum is the main monocot species planted on the front dunes of both MA-4 and MA-5, with coastal blue stem observed on the backward slope of MA-4 and no other monocots observed on the entire front dunes in MA-5, as of April 2022. Front dunes in MA-4 cover approximately 352 m^2 and those in MA-5 cover approximately 253 m^2. Due to the planned replanting efforts, no dicot species were found as of April 2022 in MA-4 and MA-5.
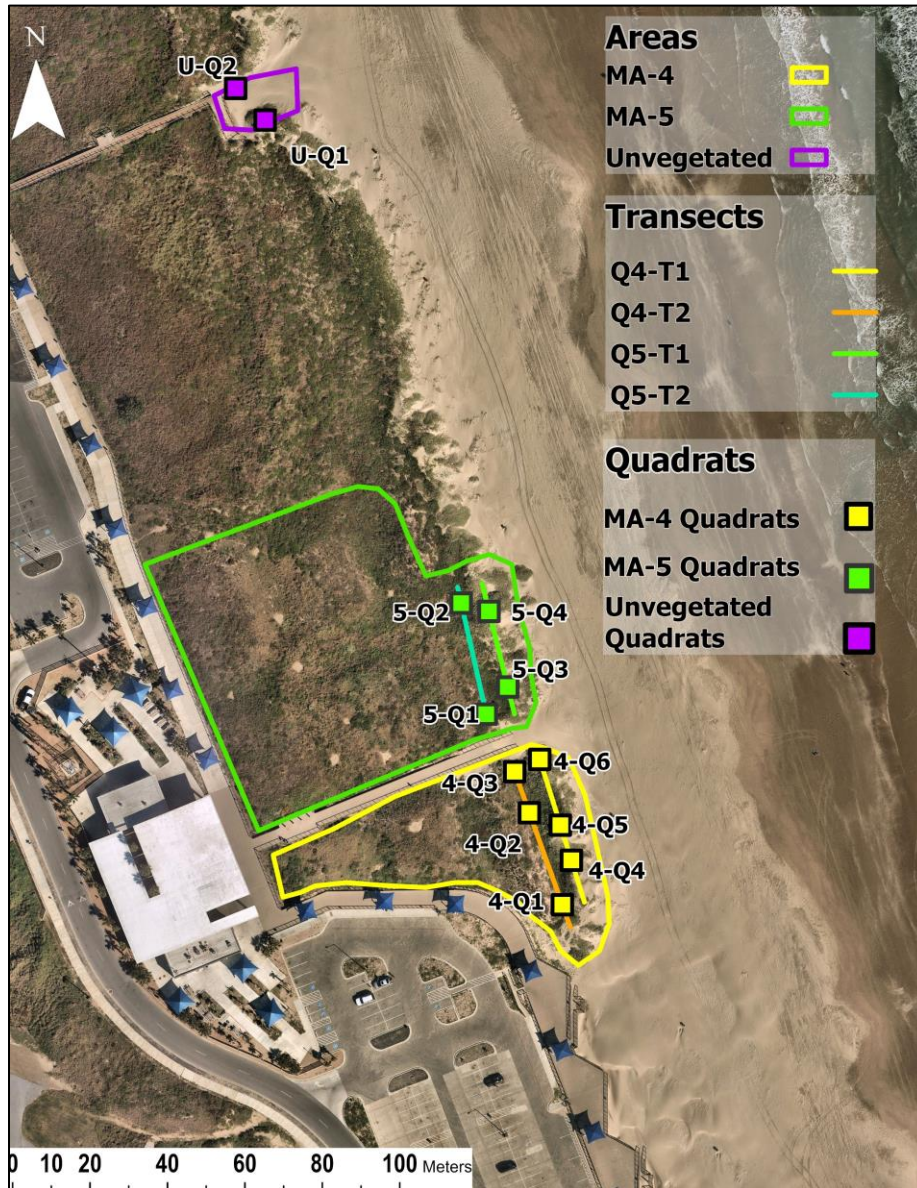
Figure 2.2: Quadrats for in-situ data collection in MA-4 and MA-5 of Isla Blanca Beach Park, SPI, Texas, USA. Notation for quadrats is in the form of X-QY, where X is the mitigated area number (i.e., 4 or 5), Q is the notation for quadrat, and Y is the quadrat number in the area, while U stands for unvegetated section.

2.2 Field Data Collection Methods

Data collection in MA-4 and MA-5 began in December of 2021. The front dunes of the

area were the main focus since they are the most vulnerable to erosion. The front dunes of both

mitigation areas also had the highest monocot vegetation density, as a result of transplanting

during restoration. Figure 2.2 shows a map of quadrats used for sampling including six quadrats

in MA-4 (4-Q1 to 4-Q6), four quadrats in MA-5 (5-Q1 to 5-Q4), and two quadrats in the

unvegetated section (U-Q1 and U-Q2). The two quadrats, U-Q1 and U-Q2, were selected to

collect unvegetated sediment data in December 2021 and September 2022 and to compare the

performance of sediments with and without vegetation.

From December 2021 to March 2023, vegetation density assessments were conducted to

measure overall vegetation density and that by plant species (i.e., monocot and dicot) followed

by the measurement of in-situ shear strength of sediment. Soil core samples were collected in the

quadrats to determine root length density and particle size distribution of the sediment after a

shear test. Data was collected every three months initially in December 2021, March 2022, and

June 2022. An adjustment in the data collection interval was made during the summer of 2022 to

collect data every six weeks, and we also collected data in the event of storms or other events on

August 4th, 2022, and September 30th, 2022. The last two data sets were collected in December

2022 and March 2023. Transect lines for quadrats were initially along one line on top of the

dunes in December 2021, but a second transect was added along the dune slopes in the following

site visits to provide better description of dune dynamics (Figure 2.2).

Quadrat sampling method (Cox, 1990) with size of 1 m × 1 m (Figure 2.3) was used

along two transect lines on the foredunes in MA-4 and MA-5 (Figure 2.2) to assess vegetation

density. The locations of quadrats were determined along the transect line, approximately one

quadrat per 10 meters. Data was collected at three quadrats per transect in MA-4 with a horizontal foredune length of 32 m, and two quadrats per transect line in MA-5 with length of 23 m. The number of plants was counted by species, i.e., monocot and dicot.

To determine the Root Length Density (RLD), soil samples were collected at the site using a soil core sampler with a 0.5 m ×0.5 m auger blade. Initial soil cores contained little to no materials with dead grass and wind blow plant matter, therefore subsequent sampling was adjusted by removing 0.2 m of topsoil before sampling at each quadrat. Soil samples from each quadrat were sorted and visible monocot roots were selected. The roots of the dicots observed were very fine and broke easily during core sampling, making it hard to accurately assess their length. The total length of roots measured was divided by the volume of the soil sample to determine the root length density at each quadrat.

Figure 2.3: Quadrat sampling (size: 1 m × 1 m) for vegetation density assessment.

In addition to the vegetation data collected in the field, the 30-m resolution Landsat satellite Normalized Difference Vegetation Index (NDVI) data was also obtained for the period of Jan 1, 2016 - Dec 31, 2021, to understand the overall improvement in vegetation growth in each of the restored areas.

2.3 Statistical Analysis

ANOVA single factor analysis was conducted to evaluate the variations in the vegetation density, the RLD, and the % monocot coverage between data collection dates and among quadrats. Before the ANOVA analysis, the data sets underwent normality and equal variance tests. The Ryan-Joiner test, a test similar to Shapiro-Wilk, was used in Mintab 17 (Minitab, LLC) to determine if the data sets followed a normal distribution. If the data set was considered normal, it was then tested for equal variance using Bartlett's test in Minitab 17. For the data sets that passed both the normality and the equal variance tests, the ANOVA single factor analyses were conducted in Excel. In addition, to further elucidate the factors contributing to the temporal and spatial variations of the vegetation data, correlations with precipitation for both rainfall data close to the sampling dates in the same month and in the month before the sampling dates were conducted. The correlation analyses were conducted using Excel. A significance level (alpha) of 0.05 was used in all statistical analyses conducted.

2.4 Results

2.4.1 Precipitation

The precipitation data retrieved at the Brownsville weather station near Cameron County, Texas is presented in Figure 2.4. Despite a yearly variation over the study period, a specific pattern in monthly precipitation was observed. That is, precipitation in May and September is relatively higher than the rest of the months in each year, which is consistent with the expected low precipitation in winter and early spring (November 2022 to March 2023) in the study region.
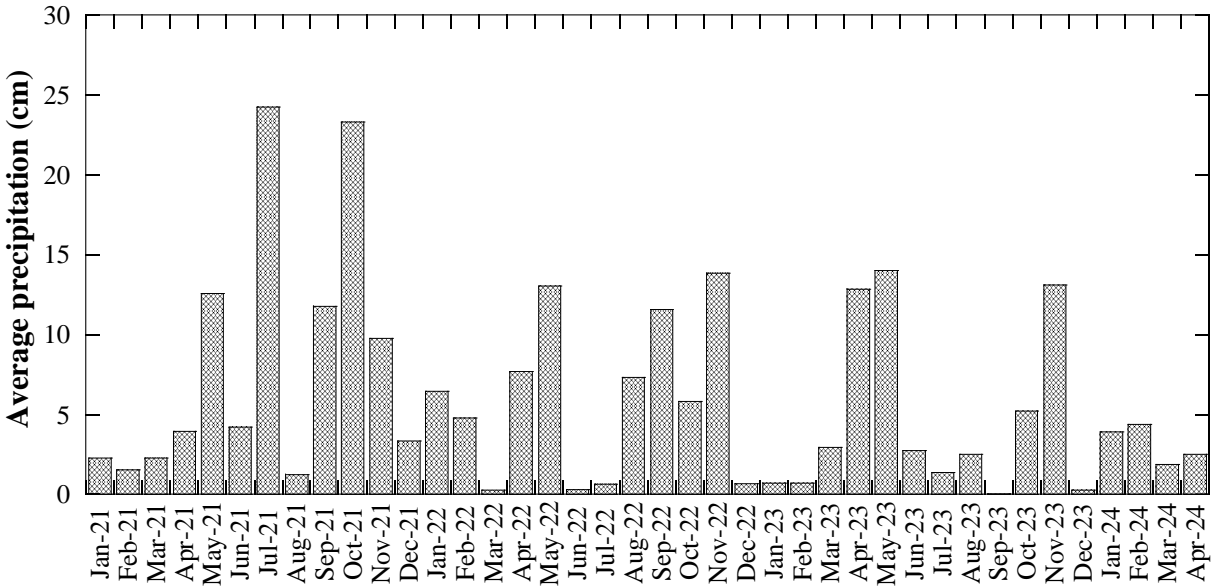
Figure 2.4: Precipitation in Brownsville, Cameron County, Texas. (NOAA National Center for Environmental Information, 2022).

2.4.2 Vegetation Density

In the mitigated areas, MA-4 and MA-5 (Figure 2.2), in general, monocot species (e.g., bitter panicum, sea oats, marshhay cordgrass, coastal bluestem) were observed on the top of the dunes whereas dicot species (e.g., gulf croton, road vines, beach morning glory, and camphor weed) at the toe of the dunes. The acquired vegetation density data is classified into three categories: overall vegetation density (hereafter vegetation density), monocot density, and dicot density. Note that vegetation density is the sum of the monocot and dicot densities. The vegetation density was higher at MA-4 than that at MA-5 (Figure 2.5) and both MA-4 and MA-5 have much higher vegetation density than the unvegetated areas at U-Q1 and U-Q2. Although it is hard to identify a general trend in vegetation density over the study period, it was observed that the vegetation densities are generally higher during the rainy season (March through

September), especially at MA-4. All vegetation observed at U-Q1 and U-Q2 belongs to the dicot species.
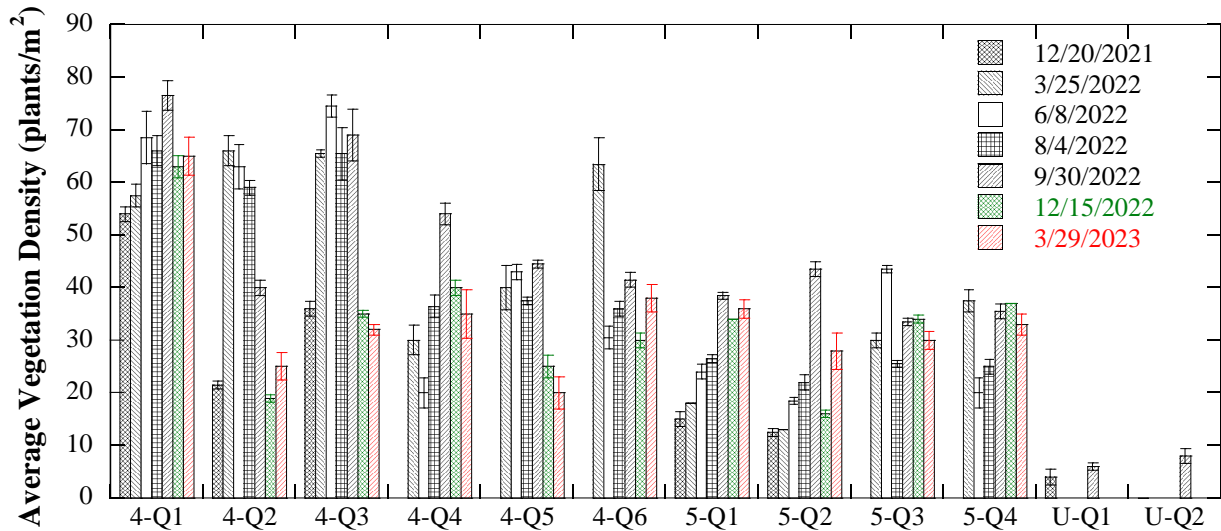
Figure 2.5: Vegetation density (combining monocot and dicot densities) across MA-4, MA-5, and unvegetated dunes. Error bars indicate standard deviation in 2 vegetation density measurements at individual quadrats.

Figure 2.6 shows the contribution of monocot and dicot species to the overall vegetation density. Monocots contributed to more than half of the vegetation density in seven out of ten quadrats in the mitigated areas in March 2022, six quadrats in June 2022, eight quadrats in August 2022, nine quadrats in September 2022, eight quadrats in December 2022, and seven quadrats in May 2023. Dicot species account for the remainder of vegetation density, with an entirely natural origin after the restoration in 2020 with the transplant of only monocot species. Thus, the contribution of dicot species to the overall vegetation density is maintained constant although it is not dominant.

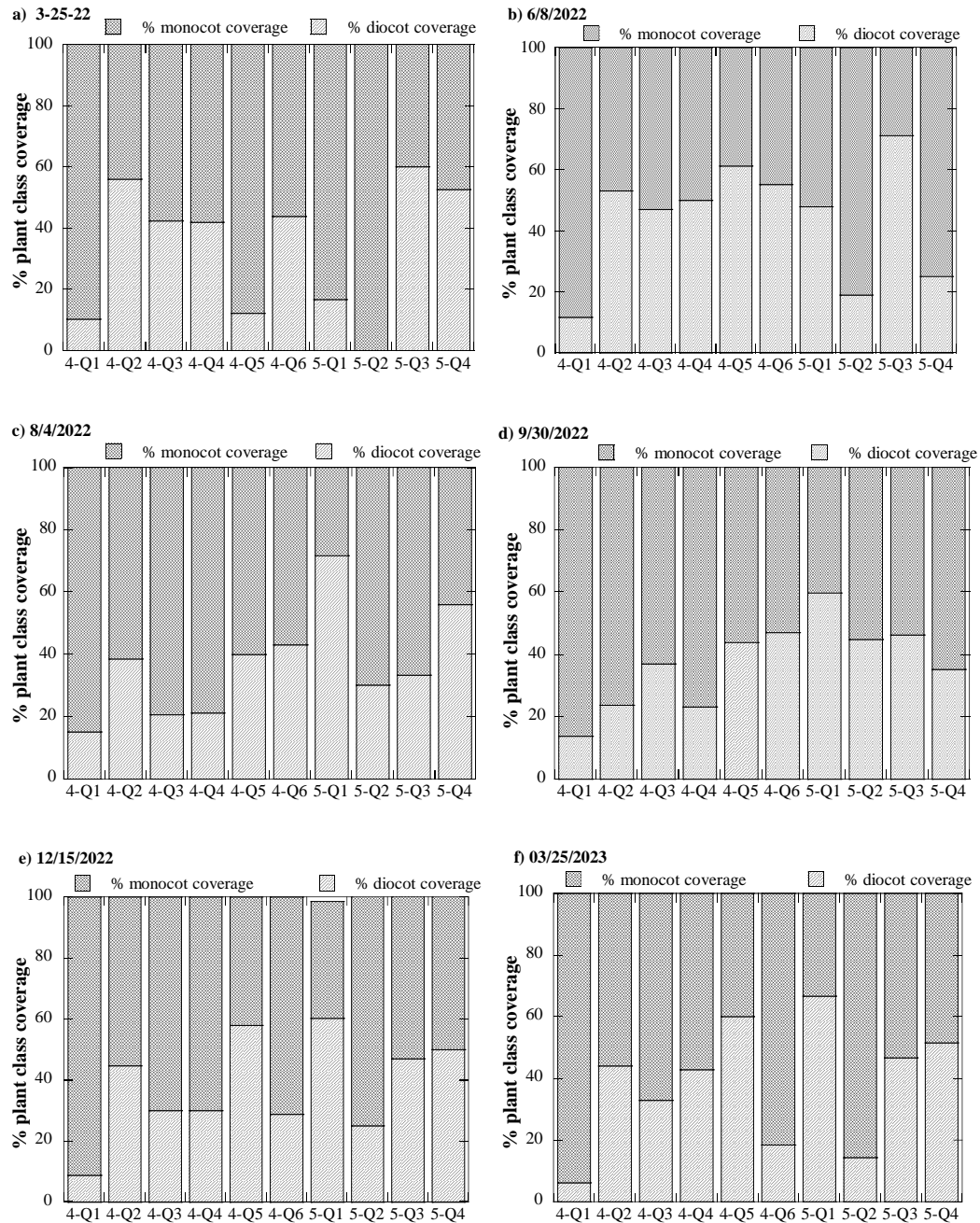Figure 2.6: Percent vegetation density by plant class across MA-4 and MA-5 based on two density measurements at individual quadrats: (a) March 2022, (b) June 2022, (c) August 2022, (d) September 2022, e) December 2022, and f) March 2023.

2.4.3 Root Length Density (RLD)

As mentioned above, RLD from each soil core sample was determined based on the monocot roots observed in each core sample, due to difficulties in identifying the roots of dicot species. Note that RLD in Figure 2.7 does not mirror the vegetation density in Figure 2.5 since roots may remain for a while in soil even after plants die due to reasons such as continued low precipitation. In other words, the RLD may not necessarily reflect above ground vegetation, suggesting the above and below-ground systems may be counted independently of each other.
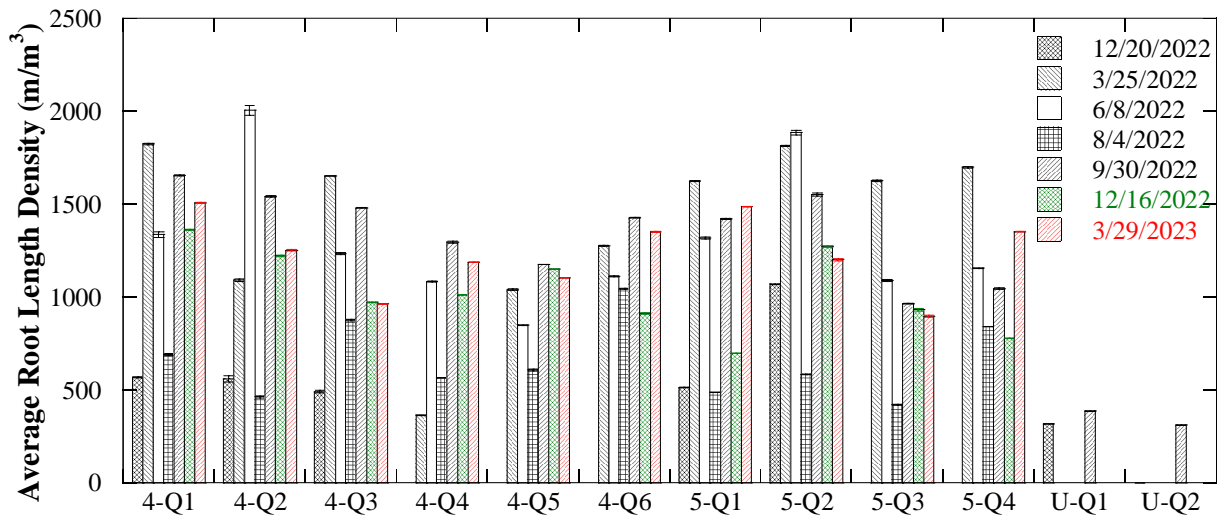
Figure 2.7: Root length density across MA-4, MA-5, and unvegetated dunes.

The RLD at all quadrats in August 2022 exhibited relatively low values (Figure 2.7) compared to those in other months, which is consistent with the relatively low vegetation density in August 2022 (Figure 2.5). This low RLD and vegetation density might result from the low precipitation in June to July 2022 (Figure 2.4). Unvegetated dunes (U-Q1 and U-Q2) presented lower RLD in December 2021 and September 2022, despite an increase in dicot vegetation density visually observed in September 2022. Please note that there were no monocot roots at U-Q1 and U-Q2, so the RLD observed at U-Q1 and U-Q2 are all dicot roots.

2.4.4 Normalized Difference Vegetation Index (NDVI)

Table 2.1 shows the annual average NDVI values and Figure 2.8 shows the monthly

NDVI values. The NDVI values increased over time, with continuous increases observed starting

fall 2019. This seems to coincide with the dune restoration effort conducted at the study site

around that time.

Table 2.1: Average annual NDVI (dimensionless number) (Data extracted by Arushi Khare and

Adnan Rajib).

Site	2016	2017	2018	2019	2020	2021
MA-2	0.14	0.13	0.17	0.18	0.23	0.23
MA-4	0.08	0.08	0.09	0.13	0.26	0.26
MA-5	0.13	0.14	0.12	0.18	0.35	0.32
MA-6	0.15	0.14	0.14	0.11	0.24	0.22
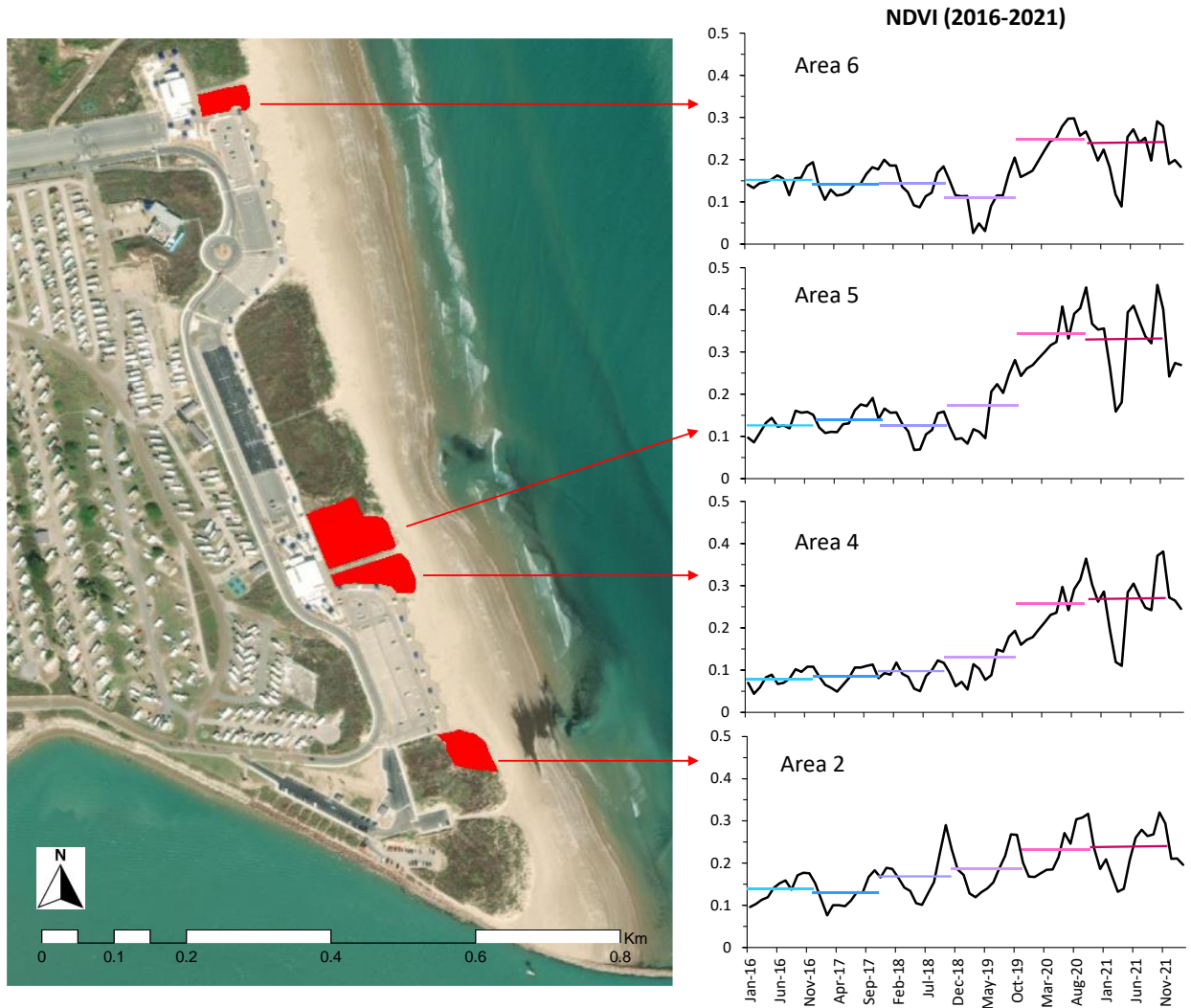
Figure 2.8: Trend of monthly NDVI (dimensionless number) for the period of Jan 1, 2016 - Dec 31, 2021. (Data extracted by and plot prepared by Arushi Khare and Adnan Rajib).

2.4.5 Statistical analysis

ANOVA analysis results indicate that there is a significant difference in vegetation density and % monocot coverage among quadrats locations, but not between sampling dates (Table 2.2). For RLD, a significant difference was found between sampling dates, but not among quadrat locations. Despite the significance in variations of RLD over time indicated by the ANOVA analysis, no strong correlations were found between the RLD and the rainfall data

(Figure 2.9). In contrast, a stronger correlation between the precipitation and the vegetation density and % monocot coverage was observed. Recall that only monthly precipitation data retrievable at the Brownsville site was available during most of the study period. Thus, direct measurements of daily precipitation at the study site in future studies might help improve the understanding of the relationship between precipitation and vegetation data.

Table 2.2: ANOVA test results.

Data types	F	F_{crit}
Vegetation Density		
Between data collection dates[1]	0.77	2.61
Among quadrats	***7.06[3]***	***2.06[3]***
Root length density (RLD)		
Between data collection dates[2]	***12.89[3]***	***2.58[3]***
Among quadrats	0.68	2.06
% monocot coverage		
Between data collection dates	0.35	2.38
Among quadrats	***5.66[3]***	***2.07[3]***

[1]Not include 09/30/2022 and 03/29/2023 data because the data did not pass the normality test;
[2]Not include 12/20/2021 and 03/25/2023 data because the data did not pass the normality test;
[3]indicate significant difference at a significance level of 0.05.
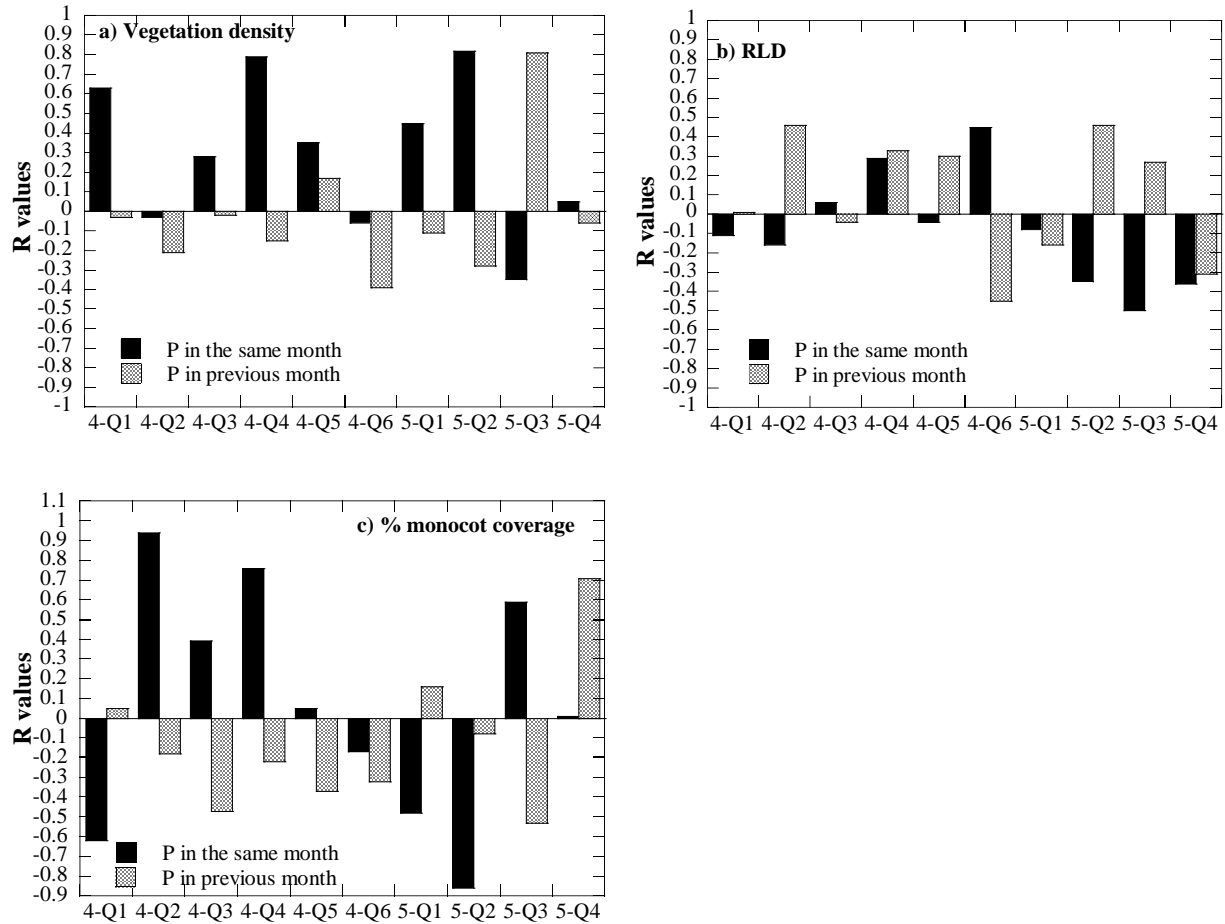
Figure 2.9: Correlations between vegetation and precipitation.

2.5 Conclusions

In this part of the work, data on vegetation density, root length density, % vegetation species coverage, and NDVI were collected and their temporal and spatial variations and correlations with precipitations were evaluated. Results show that the vegetation densities are generally higher during the rainy season (March through September), which is consistent with the stronger correlation found between the precipitation and the vegetation density. Monocot species are more prevalent than the dicot species and their coverage (i.e., % monocot coverage) also exhibits a stronger correlation with precipitation than vegetation density and RLD. NDVI is

a promising indicator for long term continuous vegetation monitoring and can be explored more in future studies. The spatial variability of vegetation density and % monocot coverage is found to be significant and the RLD variability is significant with respect to time only.

Chapter 3. Dune Shear Strength and Resilience Assessment

Vegetation has root systems that may entrap soil aggregates (Patel, 2020) and consequentially, promote dune growth. Interactions of vegetation roots and soil particles result in (apparent) soil cohesion (Wu et al., 1988), which improves the apparent shear strength of sediment. Quantifying the contribution of various species of above and below ground vegetation coverage to soil cohesion and how this affects dune growth and morphology can assist in the design of coastal dunes along the Texas coastline. This chapter describes the measurements and results of dune shear strength and the correlation between soil cohesion and vegetation factors of restored dunes at Isla Blanca Park, SPI. In addition, the relationship between dune morphology and apparent shear strength is discussed to assess how dune growth can be maintained using native vegetation.

3.1 Shear Strength Measurement Theory

Failure of soil without reinforcement is typically determined by Mohr-Coulomb criterion as follows:

$$\tau_f = c + \sigma_n' \tan \phi \qquad (3.1)$$

where τ_f is the shear strength of soil, c the cohesion of soil, σ_n' the effective normal stress on a shear failure surface, and ϕ the internal friction angle of soil. Equation (3.1) indicates that soil particles develop inter-particle friction due to confining from the effective normal stress (σ_n') to resist the shear stress on the potential (shear) failure surface. The vegetation roots in soil produce a soil-vegetation root matrix, behaving similarly to a reinforced earth with fiber, resulting in a greater shear strength than that of soil without vegetation (Simon and Collison, 2001; Ali and Normaniza, 2008). In other words, the displacement of soil particles along a potential (shear) failure surface produces shear stress acting axially on the surface of the vegetation roots across

the failure surface while the roots support the shear stress by developing tensile stress in their axial direction (Waldron, 1977).

It has been reported from several laboratory tests that vegetation roots provide extra (apparent) shear strength (ΔS_r) in addition to the shear strength (τ_f) in Equation (3.1), contributing to the shear strength enhancement without significantly changing the internal friction angle of the soil-root matrix (Gray and Leiser, 1982; Ali and Normaniza, 2008). Therefore, the Modified Mohr-Coulomb criterion of soil with vegetation roots is expressed as (Waldron, 1977):

$$\tau_r = c + \Delta S_r + \sigma_n' \tan \phi \tag{3.2}$$

Theoretically, the area ratio of vegetation roots (i.e., the sum of the cross-sectional area of roots per a unit cross-section of sediment) is one of the main parameters affecting the enhanced shear strength, ΔS_r (Waldron, 1977; Waldron and Dakessian, 1981). However, it is very hard to directly determine the area ratio in the field, so vegetation density (number of plants per unit surface area of sediment) is assessed as an alternative in this study as an analogue.

In the field tests, the shear strength of sediment with vegetation roots has been measured with in-situ direct shear testing machines (e.g., Wu et al., 1988; MacDonald et al., 2012; Fan and Su, 2008; Yildiz et al., 2018), but the measurement procedure is quite time-consuming and labor-intensive, requiring excavation of soil to set up a soil block and installation of a shear box. Furthermore, currently, there is no standard testing method (Reubens et al., 2007). Therefore, quantitative research on the role of roots in enhancing the in-situ shear strength of vegetated sediment has been limited, primarily because of methodological difficulties.

As an alternative to in-situ direct shear tests, an in-situ vane shear test has been proposed (MacDonald et al., 2012; Wieder and Shoop, 2017; Ajedegba et al., 2019) to measure the shear

strength of vegetated sediments at shallow depth (≤ 1.0 m) with higher efficiency. In a vane

shear test for unvegetated sediments, an apparatus with four vanes is inserted into the soil, and

torque is applied at the top of the rod. By rotating the rod at a constant angular speed ($\sim 0.1°$/sec),

the required torque for the rotation is measured and the shear strength (S) of soil is calculated as

(ASTM, 2008):

$$S = \frac{T}{\left(\frac{\pi}{10^6}\right)\left[\left(\frac{D^2 H}{2}\right) + \left(\frac{D^3}{6}\right)\right]}$$ (3.3)

where T is the torque in N·m, D is the diameter of the vane in cm, and H is the height of the vane

in cm.

In general, the vane shear test is used to measure the undrained shear strength of cohesive

soils (i.e., clay) while there have been several attempts to apply the method for sandy soils

(Farrent, 1960; Barros and Barros, 1989; Park et al., 2016). In this study, we measured the shear

strength of sediments with and without vegetation to assess the impact of vegetation roots on the

enhancement of sediment shear strength instead of investigating the fundamental mechanism of

the reinforcement of soil particles with the root system. As mentioned in the following section,

the soil classification of the sediment in the study area is fine sand. In general, sandy soil has

zero cohesion (c = 0) in Equations (3.1) and (3.2), so the measured shear strength with the vane

shear test comes from the frictional resistance between sand particles across the failure surface

due to the rotation of the vanes. Therefore, the difference of the vane shear test with and without

vegetation can be interpreted as the extra shear strength (ΔS_r) in Equation (3.2); i.e., the

contribution of vegetation roots to the shear strength enhancement. On the other hand, Osman

and Barakbah (2006) reported that root length density (RLD), the total length of roots per unit

sediment volume, exhibits a high positive relationship with the shear strength of sediment, but

they did not compare the impact of RLD with that of other vegetation factors (e.g., vegetation density). Therefore, this study will compare the contribution of vegetation density and RLD to the shear strength of vegetated sediment and will determine the dominant one using statistical methods.

3.2 Apparent Soil Shear Strength Measurements

We measured the in-situ shear strength of sediment with a Geonor H-60 field shear vane, with four 20 mm × 40 mm blades. As mentioned above, we measured the shear strength of sediment at locations with and without vegetation following the ASTM D 2573-08 method although it is a standard method for (cohesive) soil without vegetation, not that with vegetation. The device was inserted perpendicular into the ground at approximately 0.5 m at each quadrat (Figure 2.2) and then the handle was turned slowly until failure was observed when a click was heard. Measurements were repeated twice at each quadrat and an average was taken. During summer months when the soil was harder, in-situ apparent shear strength was harder to accurately assess in some quadrats as the vane blade could not penetrate past 0.3 m, so the readings were only collected at depths up to 0.3 m.

3.3 Laboratory Tests

After in-situ measurement of apparent shear strength, soil samples were collected using a soil core sampler with 0.5 m × 0.5 m auger blade after removing 0.2 m of topsoil before sampling at each quadrat. Sieve analysis was conducted with soil core samples acquired in every two site visits (December 2021, June 2022, and October 2022) assuming that particle size distribution of the sediments in the study area does not change rapidly over a 6-month period. A standard sieve analysis following ASTM D422-63 was employed. As a first step, samples were dried at 250 °F, and then sieve analysis was conducted with the dry samples using standard

sieves. The % mass of soil retained and the cumulative % mass retained were calculated to determine the % finer (ASTM, 2015).

3.4 Statistical Data Analysis

Based on the acquired data, we used statistical methods to identify a dominant parameter (related to vegetation) for the shear strength of vegetated sediment. More specifically, we compared the contributions of vegetation density and RLD to the sediment shear strength by determining the correlation coefficient (i.e., R-value). Thus, a parameter having a stronger correlation with the shear strength can be interpreted as a dominant one determining the shear strength.

3.5 Results

3.5.1 Particle Size Distribution

Figure 3.1 presents the particle size distributions (PSDs) of core samples. It shows that there is no significant change in the PSDs over the study period. Furthermore, particle size distribution curves of core samples acquired at separate quadrats look quite similar, suggesting that the particle size distribution of sediment in MA-4 and MA-5 is more or less homogeneous. The results of the sieve analysis also show that 80% to 90% of the soil was retained in sieves with an opening size of 0.15 mm (#80 sieve) for all analyses. Thus, the soil from core samples in MA-4 and MA-5 are classified as A-3, fine sand (AASHTO, 2012).
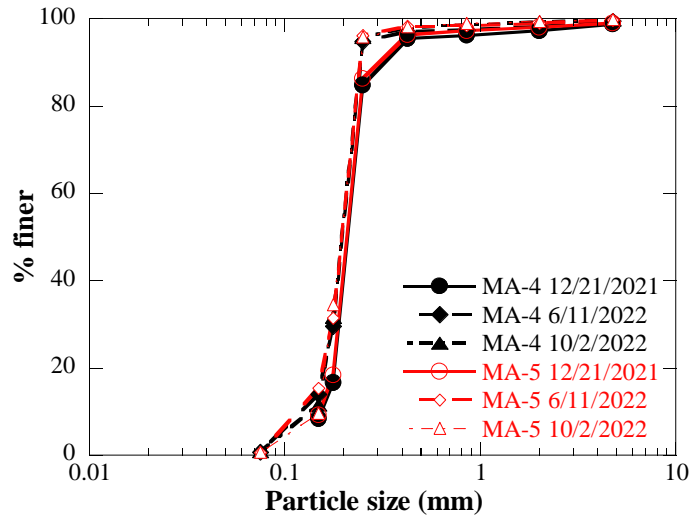
Figure 3.1: Particle size distribution for samples collected from quadrats at MA-4 and MA-5.

3.5.2 Shear Strength of Sediment

The in-situ shear strength measurements are presented in Figure 3.2. The shear strengths at U-Q1 and U-Q2 increased only slightly (≤10%) from March 2022 to September 2022. The shear strength at U-Q2 in December 2021 with zero vegetation density is 31 kPa, which is the in-situ shear strength of bare sediment (i.e., no vegetation). With this measurement, the contribution of vegetation to the shear strength can be evaluated. In December 2021, for example, the range of the measured shear strength is 46 kPa – 92 kPa which corresponds to a 48% – 200% increase in strength compared to the shear strength at U-Q2 (31 kPa) measured on the same day. This comparison confirms that vegetation increases the shear strength of sediment (e.g., Simon and Collison, 2001; Ali and Normaniza, 2008; Ajedegba et al., 2019). Although field data in this work shows that vegetation contributes to the shear strength of sediment, it is hard to directly identify a specific pattern of its changes with time and determine the dominant factor (i.e., either vegetation density or RLD) that makes a greater contribution to the shear strength enhancement

based on Figure 3.2. Thus, further statistical methods were applied, and details were described in the following section.
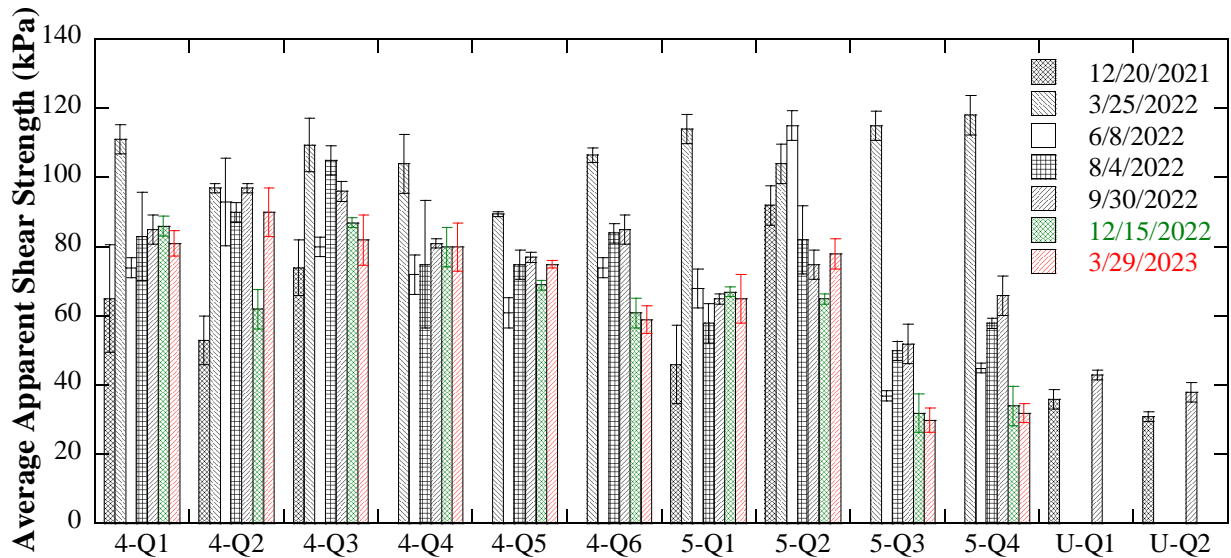

Figure 3.2: In-situ apparent shear strength measurements across MA-4, MA-5, and unvegetated dunes for all dates. Error bars indicate standard deviation in 2 overall apparent shear strength measurements at individual quadrats.

3.5.3 Relationship between Apparent Shear Strength and Observed Vegetation Parameters

The correlations of shear strength with (overall) vegetation density, monocot density, dicot density, and RLD are presented in Figure 3.3. The correlation coefficients (hereafter R-values) of shear strength with (overall) vegetation density, monocot density, dicot density, and RLD are summarized in Table 3.1. Comparison of the R-values suggests that RLD (R = 0.52 > 0.5) has the strongest correlation with the shear strength. Although the correlations are weak, monocot density exhibits a relatively stronger correlation (R = 0.33) with shear strength than (overall) vegetation density (R = 0.29). The negative correlation between dicot density and shear strength is unexpected since it was assumed that all vegetation would contribute to apparent

35

shear strength (Figure 3.3). When individual sampling period was analyzed separately, the

correlations between the shear strength and the vegetation parameters showed a temporal

variation and RLD still shows the strongest correlations with shear strength measured (Table

3.1).
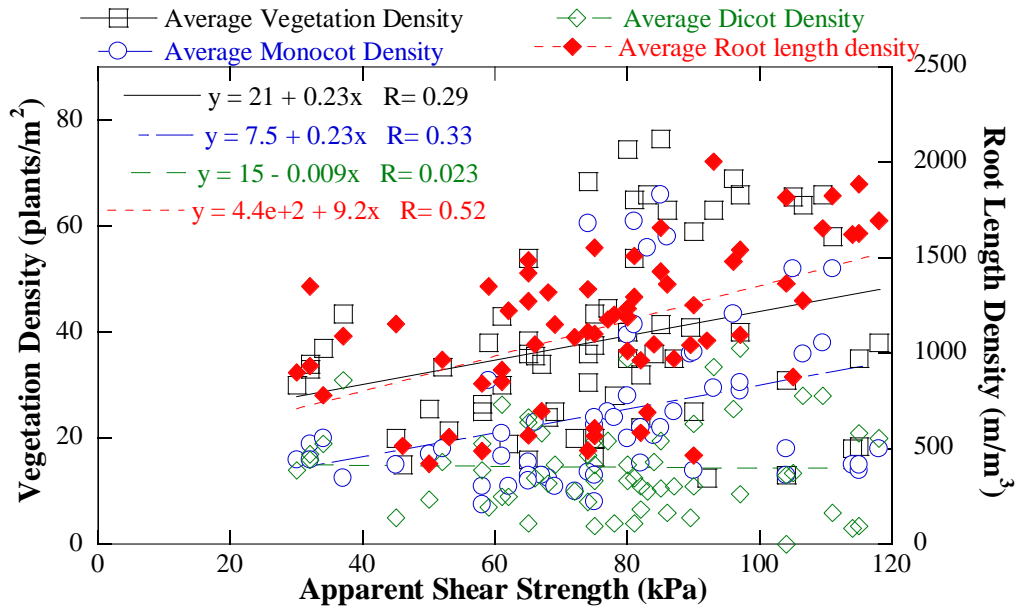
Figure3.3: Relationship between apparent shear strength and vegetation factors (overall
vegetation density, monocot density, dicot density, and root length density) at MA-4 and MA-5
for all dates.

Table 3.1: R correlations calculated for relationships between shear strength and vegetation

parameters in MA-4 and MA-5 for each data collection date.

	RLD	Vegetation Density	Monocot Density	Dicot Density
12/20/2021	**0.78**	-0.02	–	–
3/25/2022	**0.77**	-0.17	-0.26	0.02
6/8/2022	**0.76**	0.07	0.21	-0.14
8/4/2022	0.41	**0.70**	**0.72**	0.13
9/30/2022	**0.71**	**0.58**	**0.56**	-0.04
12/15/2022	0.44	0.29	0.44	-0.48
3/29/2023	0.13	0.08	0.22	-0.38

3.6 Conclusions

This study investigated the correlation between native vegetation used for restoration and sediment shear strength as an indicator of resistance of restored dunes to erosion. In-situ measurements and soil core sampling were conducted over a 15-month period to monitor above and below ground dynamics affecting the shear strength of sediment on sand dunes reinforced by vegetation. Results of the data analysis suggest that sediment with vegetation generally exhibits greater shear strength than that without vegetation. Thus, it is obvious that vegetation is a key component in coastal dune restoration to increase dunes' resilience to erosion by storms and wind. It was also found that native monocot species enhance sediment shear strength more than dicot species do, which indicates that the former should have priority in dune restoration plans over the latter. The correlations between several factors (vegetation density, vegetation density by species (i.e., monocot and dicot), and RLD) and sediment shear strength were evaluated using correlation coefficient (i.e., R-value). This analysis shows that below-ground dynamics, represented by RLD, is a dominant parameter with a greater impact on sediment shear strength compared to the contribution by vegetation density, which is consistent with previous studies.

Chapter 4. Accumulation Assessment and Data-Driven Predictive Modeling

This chapter focused on observing the changes in the terrain of the mitigated dunes at Isla Blanca Park, SPI, Texas. The work aimed at quantifying the dune volume changes using different methods. The effectiveness of the restoration methods used in this work was evaluated using Bagnold's sand transport model and data collected from topographical surveys. Bagnold's model employs a sand drift equation to calculate the sand drift rate per unit width per unit time. Wind speed, direction, and particle size of sediments are the major factors in Bagnold's model. The topographical surveys were conducted with a total station. The surveys were carried out in May and October 2020 in MA-2 which has an area of 768 m^2. MA-2 was selected because planting vegetation was completed before the study period of this work and there was no additional construction/restoration in the area afterwards. Collected data was processed using computer-aided drafting software, AutoCAD, and different sections along the foredunes and back dunes were analyzed to map the changes in the dune morphology and its volume.

4.1 Methods

4.1.1 Wind Data

Wind direction and speed are critical components in sediment transportation along the beaches. The prevailing wind conditions and characteristics of the wind in the study area (i.e., MA-2) were acquired from hourly wind data available at NOAA monitoring station 8779749. The coordinates of the station are 26°4.0 N, 97°9.3 W, located near the jetties in Brazos Santiago Pass at SPI, Texas (Figure 2.1). The station is operated and maintained by the Texas Coastal Ocean Observing Network (TCOON) and is located within a quarter mile from the study area. The station is at an elevation of 10.26 m above MSL (mean sea level), and the anemometer is at 4.24 m above the elevation of MA-2. It has sensors monitoring the water levels, winds, air

temperature, and pressure. The data is available on the "NOAA Tides and Currents" website (https://tidesandcurrents.noaa.gov/). In this study, wind data were taken hourly from May to October 2020. Pivot tables and radar graph functions in MS Excel were used to process the data. After processing the data, the frequency of wind direction and speed were identified. The wind direction was divided into 16 categories (N, NNE, NE, ENE, E, ESE, SE, SSE, S, SSW, SW, WSW, W, WNW, NW, NNW) while the speeds were split into seven categories (0-2, 2-4, 4-6, 6-8, 8-10, 10-12, >12 in m/s).

4.1.2 Topographical Surveys

In this study, a total station was used to monitor the changes in the topography of the mitigated dunes in the study area. A total station combines an electromagnetic distance-measuring instrument and electronic theodolite, which measures distance, angle, and elevation. The survey data collected using the total station has an accuracy of 1.5 mm compared to the 150 mm accuracy of the LiDAR data. Data collected using the total station is easily compatible across different data processing/modeling software platforms, which helps analyze real-world problems and develop potential solutions.

In this work, we used a Total Station, Nikon NPL 322 model, to conduct the topographical surveys. The surveys were done in the foredune and back dune regions of MA-2. Data points were collected at every 1-meter interval on the toe of the dune compared to every 3-meter interval on top of the dune. This allows more data collected at the toe of the dune to help understand the dynamics of the dune morphology since the foredune remains the most vulnerable to storm surges or high tide events.

The relative accuracy of the measurement of elevation changes on the dunes was enhanced by employing the nearest benchmark elevation that remains constant at any given point

in time. The nearest benchmark at Isla Blanca Park was located on a boulder near the jetties in Brazos Santiago Pass at SPI (Figure 2.1). The coordinates and elevation of the benchmark were retrieved from the National Geodetic Survey Data Explorer tool on the National Ocean Atmospheric Administration (NOAA) website. The benchmark is located at an elevation of 1.427 m from the mean sea level (MSL) with the coordinates of 26° 04' 05" N and 97° 09'20" W.

4.1.3 Bagnold's Aeolian Transport Model

Bagnold developed a sediment transport model after he conducted a series of wind tunnel experiments (Bagnold, 1936). Bagnold's model was the first experiment-based model and has been widely used since then. Bagnold relates sediment transportation by wind to the saltation process. Bagnold's equation suggests that the volume of sand transported is proportional to the third power of friction velocity (Bagnold, 1936). Based on his test results, Bagnold introduced a dimensionless empirical coefficient C_b based on different gradations of sand. The value of C_b ranges from 1.5 to 2.8, with the value of naturally graded sand being 1.8. Zaghloul (1992) proposed the standard diameter (D) of beach-quality sand as 0.25 mm based on experimental observations. Bagnold's equation for sand drift rate is given as follows (Bagnold, 1936):

$$q = C_b \frac{\rho_a}{g} \left(\frac{d}{D}\right)^{\frac{1}{2}} U_*^3 \tag{4.1}$$

where q = Rate of sand drift per unit width per unit time (kg/sec/m), ρ_a = Density of air (kg/m^3) g = Acceleration due to gravity (m/s^2), d = Average size of sand grain (mm), D = Standard diameter of sand (0.25 mm), C_b = Bagnold's dimensionless coefficient (Bagnold, 1936) (1.50 for nearly uniform sand,1.80 for naturally graded sand, and 2.80 for sand with broad grain size distribution), and U_*= Wind shear velocity (m/s) (Equation 4.2)

Bagnold's equation assumes that the wind flow regime on a rough surface is turbulent. When the wind velocity reaches a certain threshold (a.k.a., Wind Shear Velocity) enough to

move the sand particles, the wind velocity distribution is affected by the sand movement. The

wind velocity distribution is determined by Equation (4.2) given below (Zingg, 1952):

$$U(Z) = 6.13U_* \, log_{10} \frac{Z}{Z_t} + U_t \qquad (4.2)$$

where U(Z) = Average windspeed at height Z (m/s), Z = Height at which windspeed was taken

(m), Z_t = Fixed height above drifting surface (m), and U_t = Windspeed at height Z_t (m/s).

Equations 4.3a and 4.3b were used to calculate Z_t (modified roughness height) for

different diameters of sand particles, while U_t (windspeed at Z_t) was calculated using Equation

4.4.

$$Z_t = 0.01066 \text{ d in meters if d} \le 0.44 \text{ mm} \qquad (4.3a)$$

$$Z_t = 0.04572 \, (d)^3 \text{ in meters if d} > 0.44 \text{ mm} \qquad (4.3b)$$

$$U_t = 9.144 \text{ d s}^{-1} \text{ in meter/sec} \qquad (4.4)$$

Bagnold also developed a slope correction equation to account for the slope of the dunes.

In Bagnold's view, the upslope conditions decrease the transport rates while the downslope

conditions increase it (Bagnold, 1973). Bagnold's slope correction equation is given by

(Zaghloul, 1992):

$$q' = \frac{q}{cos\theta (tan\alpha + tan\theta)} \qquad (4.5)$$

where q' = sand drift rate on the sloping surface (kg/sec/m), q = sand drift rate calculated from

Equation 4.1 (kg/sec/m), α = angle of repose of dry sand, and θ = angle of slope of the dune. This

study used Bagnold's model to estimate the sand drift rate based on the wind direction. For the

calculation of the draft rate, we assumed that the study area is dry, and the sediment availability

is unlimited. The sand drift rate was calculated for the months of May to October 2020.

The drift rates were calculated in units of kg/sec/m and were converted into kg/month/m

and m^3/month/m. The wind data obtained from NOAA monitoring station 8779749 was analyzed

to find the prevailing wind speeds and directions and the data was used to evaluate the sand flux rates. The diameter of the sand particle at Isla Blanca Park was determined using particle size analysis (Chapter 3). The height at which the wind speed observations were conducted was at an elevation of 14.5 meters from the MSL (NOAA Tides and Currents, 2020). The slope angle (θ) of the dune was assumed to be 30°, 35°, 40°, 45°, 50°, and 55° from May to October 2020, respectively. The assumption of the angle of the dune slope was based on restoration plans and dune growth observations. The angle of the dune slope of MA-2 was determined from May to October 2020 using the onsite observations. The angle of repose of dry sand was assumed to be 34° (Hamzah and Omar, 2018). Finally, the sand drift rates for each wind direction were determined using Bagnold's equation (Equation 4.1).

4.1.4 Potential Sand Flux Model

After calculation of the sand drift rates, the volume of the sand drifted per wind direction and the category was calculated using Equation 4.6 (Zaghloul, 1992) expressed as follows:

$$Q_j = \Sigma_j \Sigma_i \, q_{ij} \cdot T_{ij} \tag{4.6}$$

where Q_j = Volumetric amount of sand drift per given direction (kg/sec/m), q = Rate of sand movement from Bagnold's equation (kg/sec/m), T = Percentage of the frequency of occurrence of wind in a certain direction and wind category, j = Standard wind directions (N, NNE, NE, ENE, E, ESE, SE, SSE, S, SSW, SW, WSW, W, WNW, NW, NNW), and i = Wind category based on wind speed (0-2 m/s, 2-4 m/s, 4-6 m/s, 6-8 m/s, 8-10 m/s, 10-12 m/s, >12m/s). In Equation (4.6), the sand drift rate (q) used was the drift rate obtained (q′) after the slope equation was corrected (Equation 4.5).

4.1.5 Methods Developed for Data Processing and Volume Change Calculations

A method was developed to determine the changes in dune morphology in 2020. Topographical surveys were performed at MA-2 of Isla Blanca Park to observe the mitigated dune volume changes. The first survey was conducted in May 2020 when the area began to trap the sand. A subsequent survey was conducted in October 2020.

Before analyzing the survey data, MA-2 was tied up to the nearest benchmark at Isla Blanca Park. The data collected from the topographical surveys was then aligned with the benchmark. The alignment of the survey data with reference to the benchmark makes it possible to observe the dune morphological changes with respect to the benchmark and MSL. The survey data was then processed using AutoCAD to determine the changes in the dune topography. Different sections along the restored dune were analyzed to account for the morphological and volumetric characteristics of the dune (Figure 4.1).

The method developed in this study consists of two parts: (i) displaying the dune morphology and (ii) evaluating its volume change. For displaying the dune morphology, two-dimensional profiles were created at different locations along the foredune and back dune using AutoCAD. The development of the two-dimensional (2D) sections was carried out for the data collected in May and October 2020. After developing the elevation profiles, a mean sectional area was generated in AutoCAD to calculate the dune volume. The mean sectional area of the dune was determined by taking an average of elevations across the whole dune section. Finally, the dune volume was calculated by multiplying the mean sectional area by the average dune profile length.
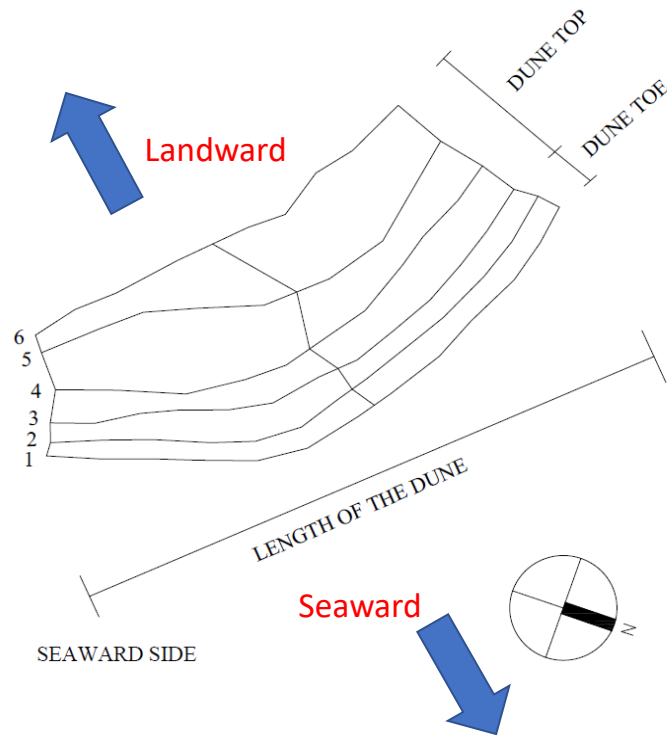
Figure 4.1: Plan View of MA-2 dune at Isla Blanca Park, SPI, Texas.

4.2 Results

4.2.1 Wind Distribution from May to October 2020

Figure 4.2 shows that the prevailing wind direction from May to October 2020 was South-South-East except for May where the wind was predominantly moving from South-East. The major wind speed category for May and June 2020 was 6-8 m/s, while the major wind speed category for July and August 2020 was 4-6 m/s. For September and October 2020, the prevailing wind speed categories were 4-6 and 6-8 m/s, respectively. The high wind speeds and change in the wind direction towards North-North-East for September 2020 can be attributed to Tropical Storm Beta (September 17-25, 2020). The calculated percentages of wind direction and speeds are used in estimating the potential sand flux rates (Equation 4.6).
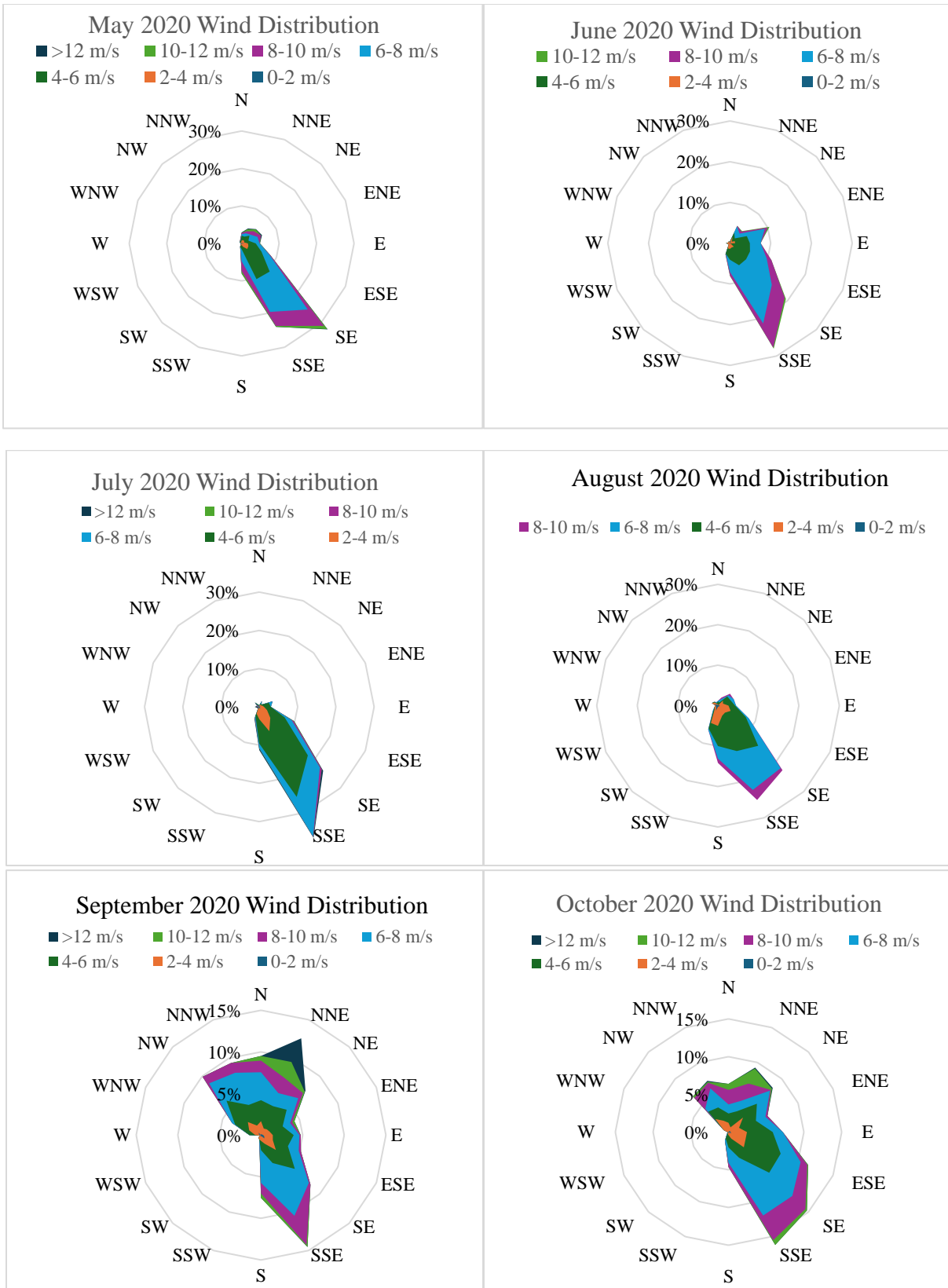
44

Figure 4.2: Wind Distribution from May to October 2020.

4.2.2 Potential Sand Flux Estimates

Figure 4.3 shows the results for potential sand flux rates from May to October 2020 at MA-2 of Isla Blanca Park using Equation 4.6 and wind data. In May, the sand flux rate was higher in the South-East direction. From June to October, the sand flux rate was higher in the South-South-East direction except for September when the sand flux was higher in the North-North-East direction.
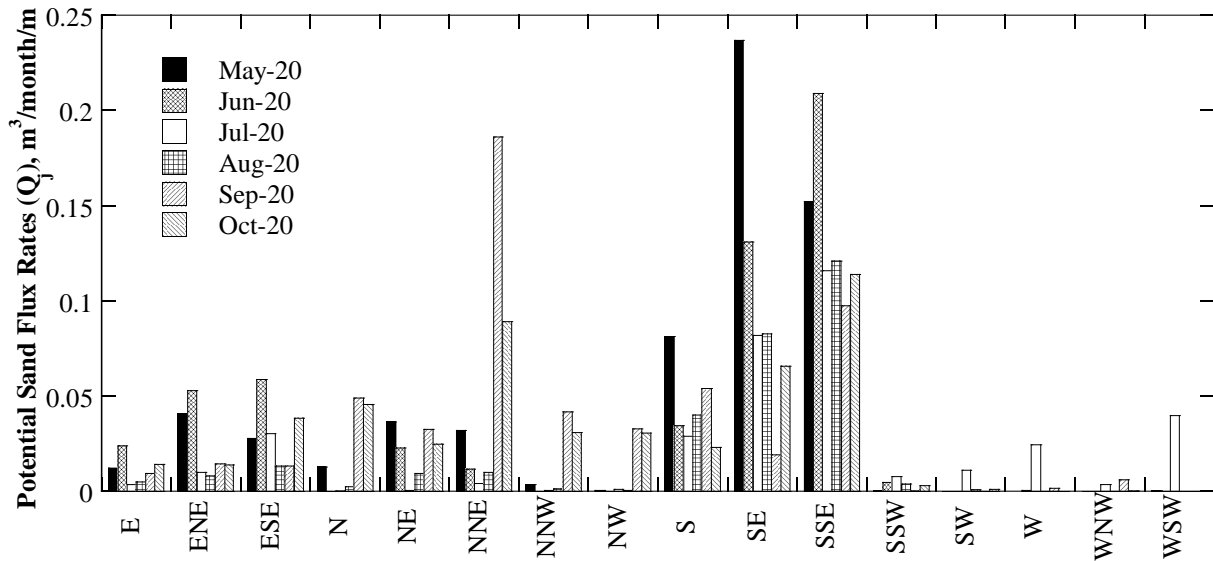

Figure 4.3: Potential Sand Flux rates at MA-2 from May to October 2020.

Figure 4.4 shows the estimated sand transport rates in all directions for MA-2 at Isla Blanca Park from May to October 2020. The sand transport rate at MA-2 was determined for each month by adding up the sand transport rate from all directions. The estimated sand transport rates in all directions from May to October 2020 were 0.64, 0.55, 0.36, 0.30, 0.56, and 0.50 in m^3/month/m. Therefore, the sum of the sand transport rates from May to October 2020 was 2.91 m^3/m.
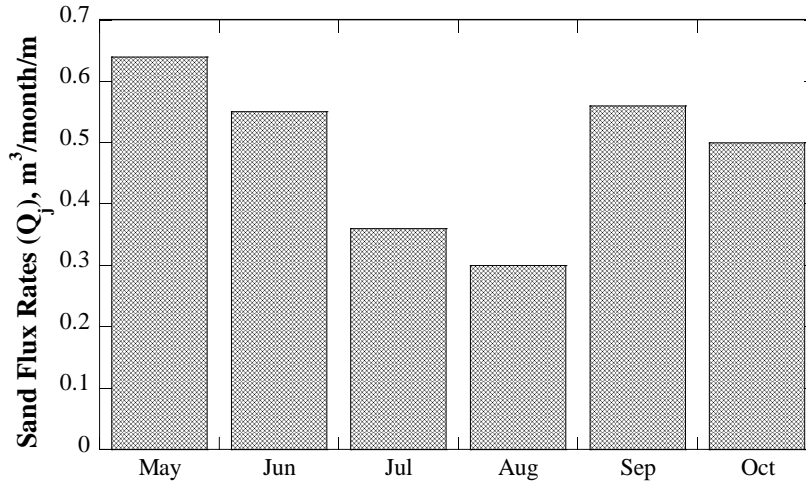
Figure 4.4: Estimated Sand Transport Rates for MA-2 at Isla Blanca Park.

4.2.3 Changes of the Dune Morphology

4.2.3.1 Comparison of Dune Elevation Profiles

The elevation profiles for lines 1 and 6 (Figure 4.1) were developed to observe the changes in the dune morphology. Figure 4.5 compares the dune elevation profiles at the toe (line 1, Figure 4.1) and top (line 6, Figure 4.1) of the dune from May and October 2020. The dune profiles were developed with reference to the nearest benchmark to the restoration areas at Isla Blanca Park. Therefore, the elevation of 0.00 in Figure 4.5 is the mean sea level. The mean elevation of the dune profiles was calculated by taking an average of all the elevations across the profile. The mean elevation of the dune toe shown in Figure 4.5 for May 2020 was 2.75 m, while the mean elevation for October 2020 was 2.86 m.

A slight increase in the level of sand can be observed on top of the dune across certain locations from May to October 2020. The mean elevation of the top of the dune for May 2020 was 5.01 m, while the mean elevation for October 2020 was 5.26 m. The increase in the level of sand on top of the dune when compared to dune toe can be attributed to the growth of vegetation and the low impact of storm surges on the back dune of the restoration area.
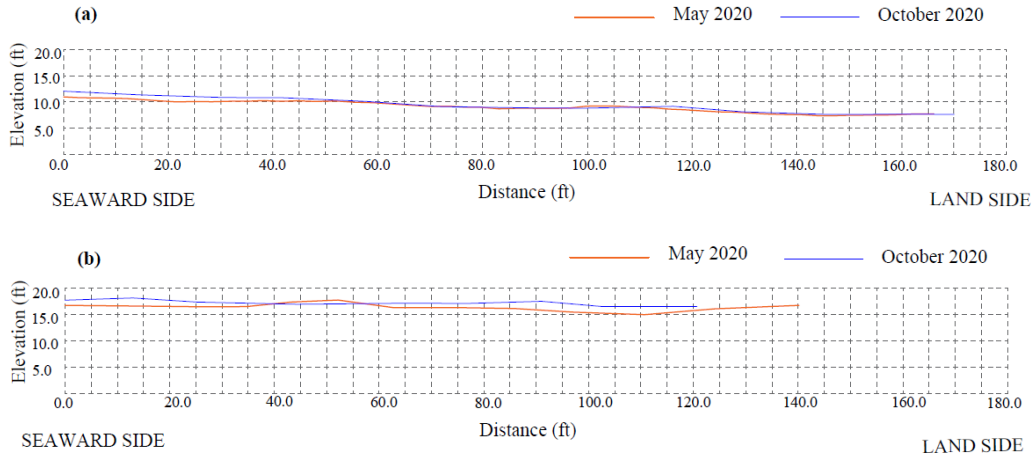
47

Figure 4.5: Comparison of elevation profiles in MA-2 for May and October 2020 at a) dune toe and b) dune top.

Based on the dune elevation profiles, a mean sectional profile was developed in AutoCAD by taking an average elevation of the dune across each section. Figure 4.6 shows a slight increase in the mean sectional profile of MA-2 from May to October 2020.
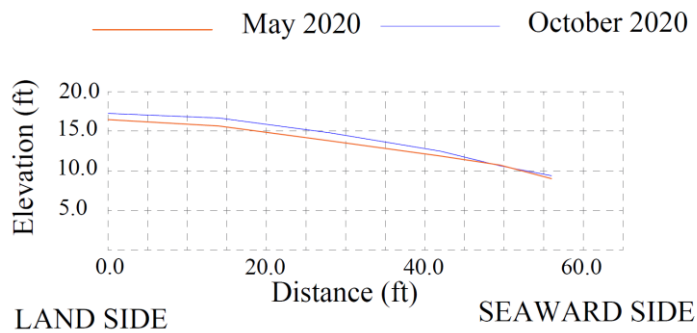

Figure 4.6: Comparison of mean sectional profiles in MA-2 for May and October 2020

4.2.3.2 Dune Volume Calculations

After generating the mean sectional profile (Figure 4.6), the area of the dune was determined using the "Area" command in AutoCAD. The area of the dune is multiplied by the

48

average dune profile length to find the dune volume. The dune volume calculations for MA-2 were conducted for May and October 2020. The volumetric calculations were performed using AutoCAD and simple mathematics. From May to October 2020, the dune volume of MA-2 increased by 179 m^3 (Table 4.1). The dune growth rate for MA-2 was calculated by dividing the dune growth volume by the average dune profile length and was found to be 3.97 m^3/m.

Table 4.1: Dune Volume Calculations for MA-2 in May and October 2020.

Description	Units	May 2020	October 2020
Area of top of the dune	m^2	56.7	60.2
Area of toe of the dune	m^2	13.8	14.1
Length of top of the dune	m	40.2	40.5
Length of toe of the dune	m	49.1	49.4
Volume for top of the dune	m^3	2,280	2,442
Volume for toe of the dune	m^3	679	696
Total dune volume	m^3	2,959	3,138

4.3 Summary and Conclusions

Coastal dunes play a critical role in reducing the effects of extreme weather events on coastal communities. Different approaches are adopted for dune stabilization across the world. Systematic planting of vegetation on the dunes has proven to be effective and is being widely adopted. Apart from dune stabilization measures, it is also essential to understand the factors affecting the growth/erosion of the dunes. Wind speed and direction are factors that play a vital role in dune growth. In this study, wind speed and direction patterns at MA-2 of Isla Blanca Park were analyzed and the sediment transport rates were calculated using Bagnold's method from

May to October 2020. The sediment transport rate from May to October 2020 was found to be 2.91 m^3/m.

An analytical method was developed to quantify the dune morphological changes at MA-2 of Isla Blanca Park. The data obtained from the topographical surveys were evaluated using AutoCAD to observe and calculate the dune volume changes. The surveys were performed in May and October 2020 at MA-2 of Isla Blanca Park. The top of the dune had higher growth compared to the toe of the dune in MA-2 which reinstates the fact that the foredune remains most vulnerable to storm surges or high-tide events. The change in dune volume from May to October 2020 was found to be 3.97 m^3/m. The difference in dune growth rate from that calculated using Bagnold's model (2.91 m^3/m) to one estimated based on the topographical survey data (3.97 m^3/m) can be attributed to factors not included in Bagnold's model, such as vegetation, temperature, precipitation, and wave characteristics. The inclusion of such factors would help better estimate sediment transport rates. During the study period, SPI has experienced storm surges from Hurricane Hanna (July 23–26, 2020), Tropical Storm Beta (September 17-25, 2020) and Hurricane Delta (October 4-12, 2020). The dune growth rate and the increase in height of dune elevation profiles in this period underline the importance of dune protection measures adopted in the area. To conclude, the dune protection methods implemented at MA-2 of Isla Blanca Park have been proven to be effective.

Chapter 5. Erosion Resilience Assessment

Coastal dunes play a crucial role in serving as a first line of defense against severe weather conditions (Abbate et al., 2019; Bonte et al., 2006). Dunes protect coastal regions by absorbing and dissipating the hydrodynamic energy produced by storm surges (Ciavola et al., 2014). They also provide essential services such as sediment deposition, water catchment and purification, habitat for wildlife, carbon sequestration, tourism, recreation, and education (Ciavola et al., 2014). Coastal dunes must maintain optimal geomorphological characteristics including height, width, and slope to successfully protect a coastal region from storm surges and floods (Ajedegba et al., 2019; USACE, 1984). Dunes' morphology and volume are directly affected by forcing mechanisms such as tidal cycles, sea level change, sediment supply, wind, wave patterns, storms, hurricanes, human activities, and ecological factors such as the type and extent of vegetation (Griggs and Reguero, 2021).

Elevation models of coastal dunes based on volumetric surveys may provide engineers and scientists with an efficient tool to evaluate their resiliency and stability against erosion from anthropogenic interventions and climate exposures (Zaghloul, 1992; Houser and Mathew, 2011). Various topographic surveying techniques (e.g., photogrammetry with aerial photographs, total station, LiDAR, etc.) have been developed. Among these methods, the total station (TS) has demonstrated accurate measurement of individual point coordinates (Lee at el., 2013). Unmanned aerial vehicles (UAVs) also demonstrate a wide range of uses in overseeing dynamic natural landscapes, such as monitoring changes in land formations and coastlines (Taddia et al., 2019; Zimmerman et al., 2020). UAVs are advantageous in mapping and surveying otherwise inaccessible areas, such as high-relief terrain or areas with dangerous vegetation and wildlife (e.g., cacti, snakes, etc.), while minimizing potential damage to the flora and fauna (Nesbit et al.,

2022). This chapter presents results on trends and patterns of sand dunes based on surveys with

TS and UAV in two mitigated areas of SPI, Cameron County, Texas.

5.1 Methods

Two surveying data sets were collected using a TS instrument and a UAV in MA-4 and

MA-6, the study areas in this work, with MA-4 having three dunes (fore dune, middle dune, and

back dune) and MA-6 having one dune (Figure 5.1).

5.1.1 Total Station (TS) Surveying

To develop Digital Elevation Model (DEM) profiles of the sand dunes and determine

their volumes, topographic surveys were carried out utilizing a TS instrument, a Nikon NPL 322

model. The benchmark selected was the nearest National Oceanic and Atmospheric

Administration (NOAA) station, situated at an elevation of 1.43 meters above mean sea level

(26° 04' 05" N and 97° 09'20" W) according to NOAA website (

https://tidesandcurrents.noaa.gov/benchmarks.html?id=8779750) (Figure 5.1). The benchmark

was used to orient the TS instrument to a new control point. When moving the instrument, a

provisional point was established by inserting a pole with a flag into the ground. The previous

control point, marked with an orange spray, was verified as a checkpoint to identify any errors

incurred during the relocation process.

Figure 5.1: Location of study and aerial overview of arrangements of the dunes, (a) location of SPI, (b) study sites, (c) MA-4 side view, (d) MA-4 front view, (e) MA-6 front view, and (f) MA-6 side view (Osiberu et al., 2024).

The TS survey was carried out along dune profiles, with the seaward beach face toe serving as the first profile (Figure 5.2). The TS instrument used has a resolution of sub-centimeter, and a pre-field site check was conducted to ensure that all necessary supplies were available. The TS operation typically requires two people, one person holds the rod measuring each point along the profile, while the other person records the northing, easting, and elevation as they appear on the instrument display. In general, 1 m spacing was used between the profile lines in the fore dunes and dune toe (orange lines in Figures 5.2a and 5.2b, respectively) and 3 m spacing in the back dunes and dune top (blue lines in Figures 5.2a and 5.2b, respectively). In addition, vegetation and elevation assessments were carried out at all checkpoints (Figures 5.2c and 5.2d). These checkpoints served as strategically positioned reference locations across the survey area, allowing for data collection and analysis. A total of 24 checkpoints were used at MA-4 and 17 at MA-6. Each checkpoint was precisely georeferenced.

Data was collected monthly for 5 months (between December 2022 and April 2023) to help understand the dynamics of the dune morphology. An average of 180 data points were collected at each site (MA-4 or MA-6) during the TS survey. The data obtained from the TS was then processed as a CSV file, used as an input file for ArcGIS 10.8.1 software, and interpolated using the inverse distance weighted (IWD) method to generate a DEM, which was then displayed and exported as shapefiles. The changes in sediment volume between selected study periods were calculated using the DEMs as input files via the Surface Difference Tool of ArcGIS following the guidelines of van der Wal (1996) and Andrews et al. (2002).
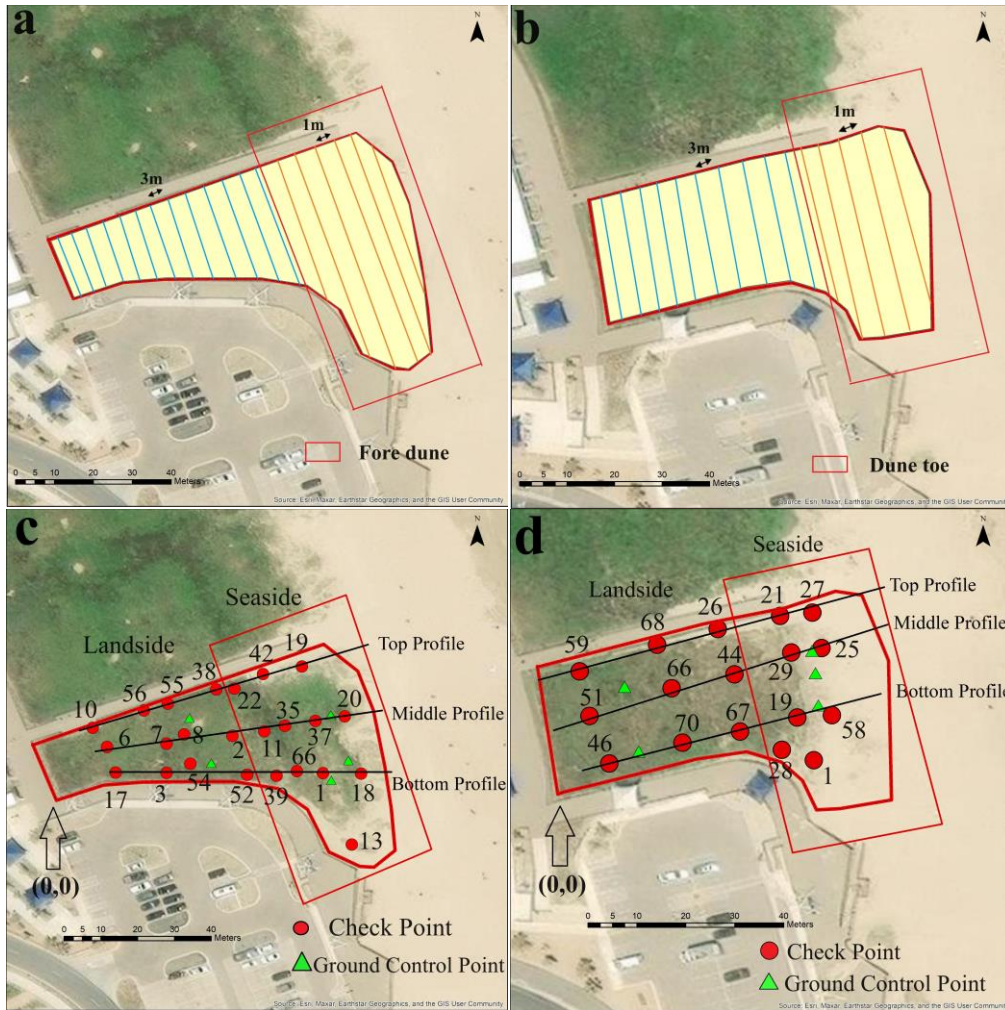
Figure 5.2: Survey profiles used for TS survey at (a) MA-4 and (b) MA-6, and checkpoints and ground control points at (c) MA-4 and (d) MA-6 (Osiberu et al., 2024).

5.1.2 UAV Survey Combined with Photogrammetry

UAV imageries were collected monthly, and the data was processed to generate DEMs based on the locations of the GCPs. A flight plan was set up in the Pix4D^{TM} Capture App. A low-weight UAV model, the ANAFI thermal, was used. To plan and oversee missions, we employed the 'Parrot' app on an Apple operating system (i.e., iOS) in the operator's cell phone, utilizing its screen for continuous monitoring of the UAV position, status, and video signal during each

flight. Each survey consisted of two 15-minute flights, taking off and landing at distinct points, to effectively cover each study area. Operating at a height of 50 meters above ground level, the UAV captured images every 2–4 seconds, implementing a double mesh overlap with latitudinal and longitudinal overlaps set at 70% and 80%, respectively. The images were taken at an average spatial resolution of 2.5 cm/pixel. This study incorporated GCPs strategically placed before each flight using a Trimble handheld receiver equipped with RTK positioning technology for enhanced accuracy. The GCPs were checkerboard wallpaper targets placed on the ground at known locations. Five GCPs were placed in each study area (Figures 5.2c and 5.2d). The GCPs were removed after flights, and flags were pegged at the known locations to avoid littering on the dunes.

Orthomosaic maps for each study area were generated through a flight plan, ensuring optimal internal camera parameters. The application of a photogrammetric process, specifically utilizing an SfM algorithm, resulted in a high-precision 3D terrain model from the UAV images. The comprehensive workflow encompassed six steps following the method of Bañón et al. (2019): (1) Incorporate Images, (2) Align Photos, (3) Position Markers, (4) Enhance Camera Alignment, (5) Develop a Dense Point Cloud, and (6) Generate DEMs.

In the initial phase, the UAV images, along with their camera positions and orientations, were embedded in the EXIF metadata of the image files. The Pix4dmapper software facilitated the identification of GCPs within overlapping image pairs during the photo-alignment process, adjusting camera positions and orientations to construct sparse point cloud models. The subsequent manual marker placement step then strategically positioned precise points across the study area to optimize camera positions and orientations, enhancing model reconstruction with the identification of visible GCPs and corresponding markers on each image.

Following this, the camera alignment optimization phase recalculated image positions using the predefined GCPs. Subsequent software steps involved the computation of depth maps for each camera, amalgamating them into cohesive dense point cloud models used to generate the DEMs. Many images (~3,000) were collected during the study period. To process these pictures obtained, PIX4D^{TM} mapper software was used to produce the orthoimages and maps. A high number of overlapping images (70% camera overlap) were used in the image processing.

5.2 Results

5.2.1 DEMs from Total Station and UAV Surveys

The DEMs generated from TS and UAV datasets show that the fore dune had the highest elevation over time in MA-4 (Figure 5.3). Also, the two valleys between the three dunes in MA-4 are clearly observed. The DEMs generated from TS and UAV for MA-4 appear to agree. MA-6 has only one dune, and the highest point was mostly observed on the dune top as captured by the TS survey except in April 2023 (Figure 5.4e), where the dune toe had the highest elevation. However, DEMs generated from UAV in MA-6 show that both the dune top and dune toe had almost the same elevation in February, March, and April 2023 (Figures 5.4h, 5.4i, and 5.4j). Thus, the DEM from UAV only fairly agrees with that from TS in this case.

To identify any significant changes in the surface topography, the changes in DEMs of MA-4 and MA-6 over time were analyzed and the results are presented in Figures 5.5 and 5.6. It was observed that there was a sand gain in MA-4 between February 2023 and April 2023 (Figures 5.5c, 5.5d, 5.5g, and 5.5h), and a loss of sand between December 2022 and February 2023 (Figures 5.5a, 5.5b, 5.5e and 5.5f). MA-6 experienced loss of sand between January 2023 to February 2023 (Figures 5.6a and 5.6e), and accumulation from February 2023 to April 2023

(Figures 5.6b to 5.6d and 5.6f to 5.6h). The elevation changes observed here show that the two survey methods produced almost the same results.
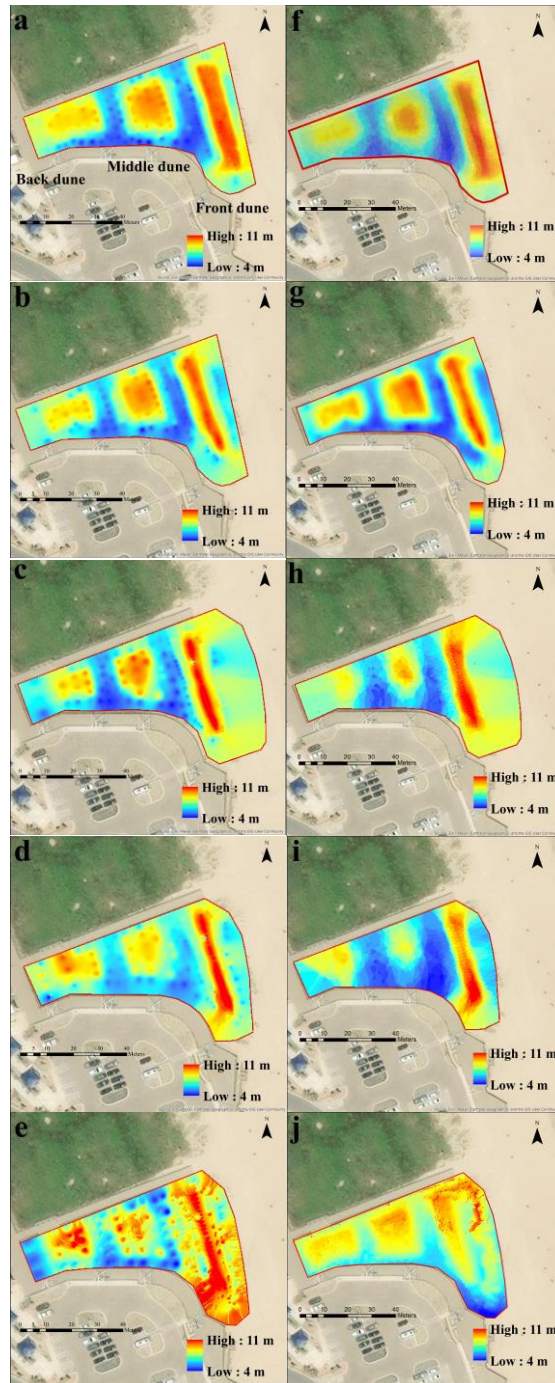

Figure 5.3: Total Station DEM of MA-4, (a) December 2022, (b) January 2023, (c) February 2023, (d) March 2023, (e) April 2023, and UAV DEM of MA-4 (f) December 2022, (g) January 2023, (h) February 2023, (i) March 2023, and (j) April 2023 (Osiberu et al., 2024).
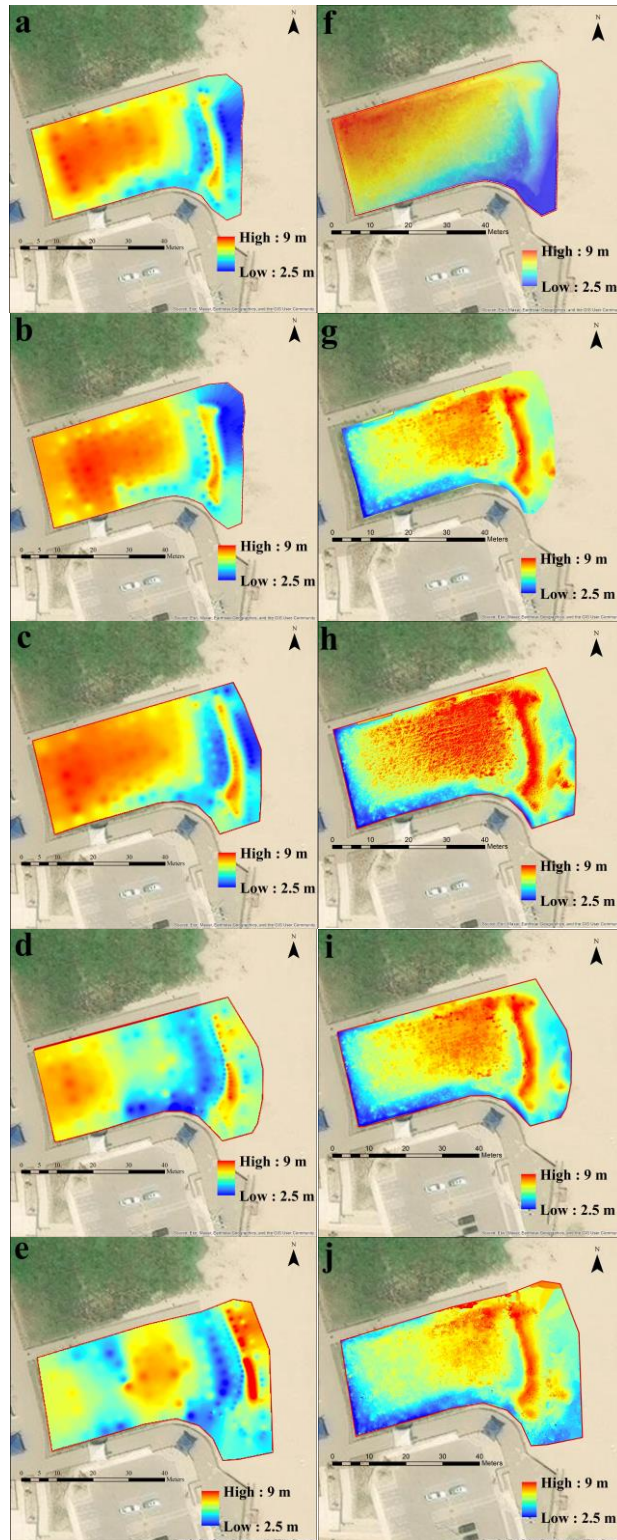
Figure 5.4: Total Station DEM of MA-6, (a) December 2022, (b) January 2023, (c) February 2023, (d) March 2023, (e) April 2023, and UAV DEM of MA-6 (f) December 2022, (g) January 2023, (h) February 2023, (i) March 2023, and (j) April 2023 (Osiberu et al., 2024).
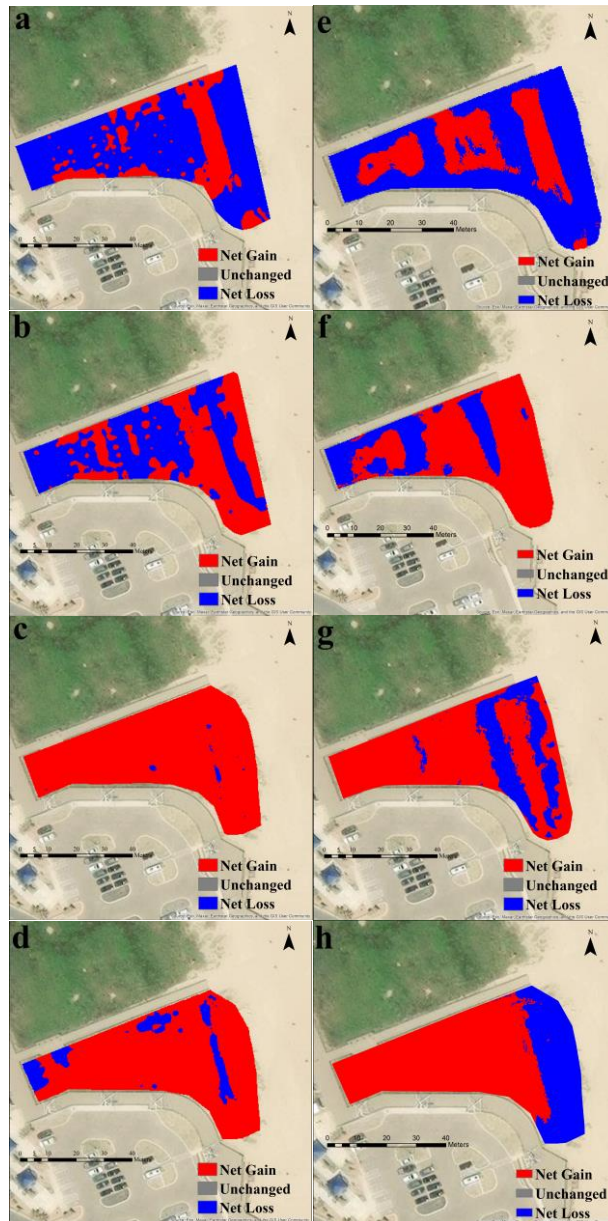
Figure 5.5: Digital model for MA-4 Total Station elevation difference, (a) December 2022-January 2023, (b) January 2023-February 2023, (c) February 2023-March 2023, (d) March 2023-April 2023 and UAV elevation difference, (e) December 2022-January 2023, (f) January 2023-February 2023, (g) February 2023-March 2023, and (h) March 2023-April 2023 (Osiberu et al., 2024).
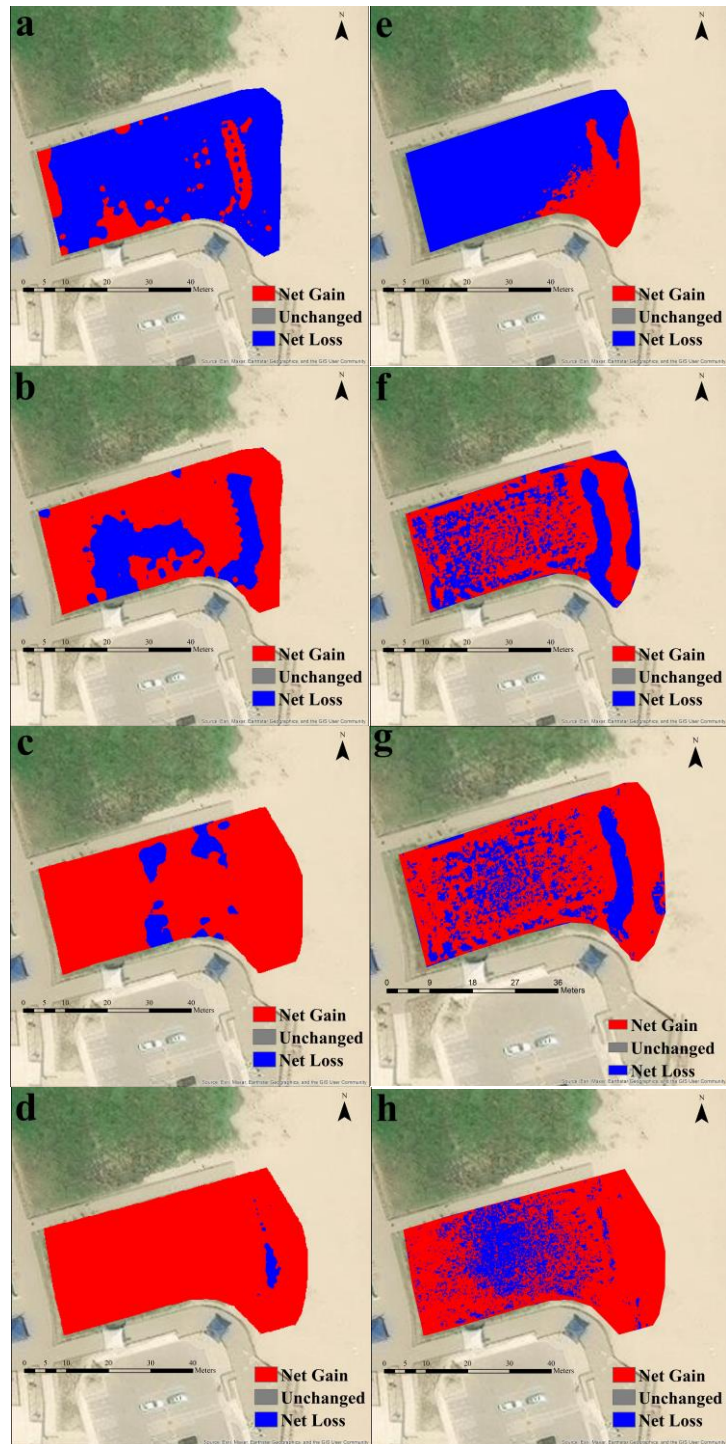
Figure 5.6: Digital model for MA-6 Total Station elevation difference, (a) December 2022-January 2023, (b) January 2023-February 2023, (c) February 2023-March 2023, (d) March 2023-April 2023 and UAV elevation difference, (e) December 2022-January 2023, (f) January 2023-February 2023, (g) February 2023-March 2023, and (h) March 2023-April 2023 (Osiberu et al., 2024).

5.2.2 Cross-shore Topographic Profiles

 2D cross-shore profiles generated from both the TS and the UAV surveys corresponding to the profile locations shown in Figures 5.2c and 5.2d were compared. The TS profiles revealed noticeable fluctuations in dune shape (Figure 5.7), especially near the seaside. The TS measurements also revealed noticeable variations in elevations across the sampling dates and a gradual accumulation of sand throughout the study period. The UAV data revealed less variation in dune morphology toward the seaside and comparable variations toward the landside. In MA-4 (Figure 5.7), both UAV and TS profiles showed an increase in dune height with time, suggesting a positive sand accumulation (i.e., growth of the dune). In MA-6 (Figure 5.8), UAV profiles remained fairly constant over time. In general, when analyzing elevation profiles obtained from the same survey methods, a consistent pattern is observed. However, there is a slight disparity when comparing elevation data collected by the two different methods. The cross-shore profiles generated from the TS appear smoother when compared to the profile obtained from the UAV. This is because the UAV has the ability to pick up more elevation points than the TS. Hence, the profile from UAV surveys can capture smaller variations.

Figure 5.7: MA-4 cross-shore profiles corresponding to profiles shown in Figure 2c. (a) TS Top-profile, (b) UAV Top-profile, (c) TS Middle-profile, (d) UAV Middle-profile, (e) TS Bottom-profile and (f) UAV Bottom-profile. Note the origin is located on the landside (Osiberu et al., 2024).
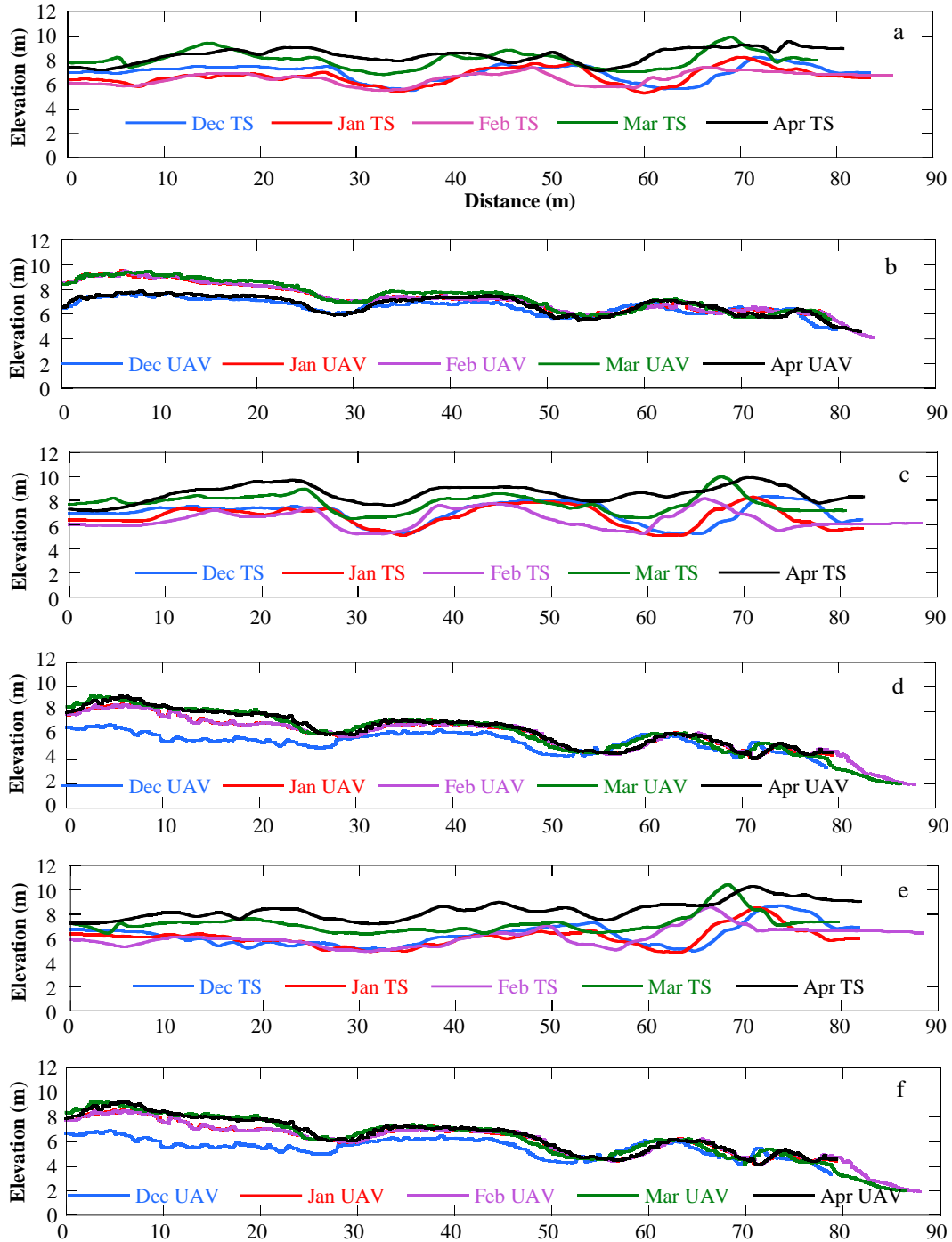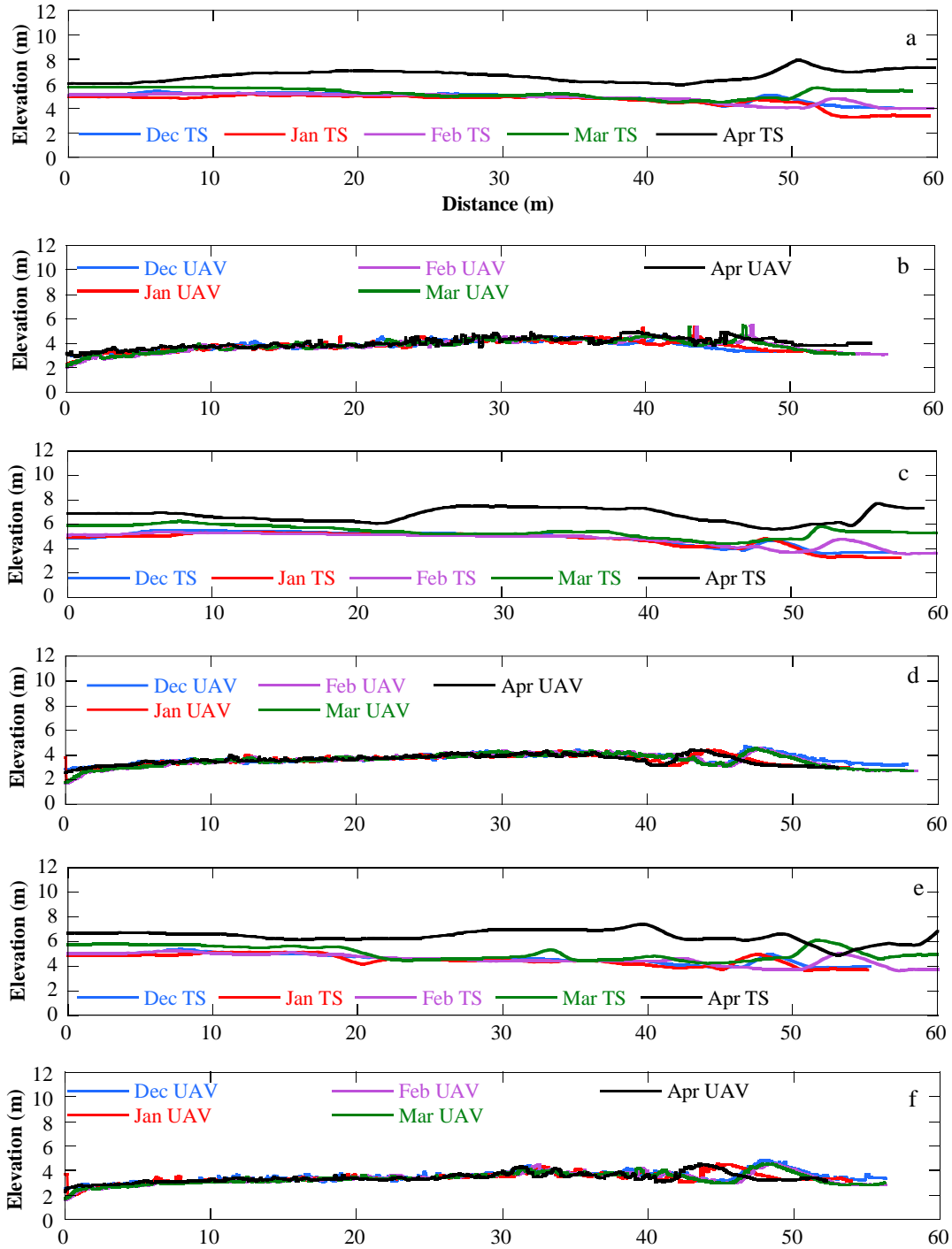
Figure 5.8: MA-6 cross-shore profiles corresponding to profiles shown in Figure 2d. (a) TS Top-profile, (b) UAV Top-profile, (c) TS Middle-profile, (d) UAV Middle-profile, (e) TS Bottom-profile and (f) UAV Bottom-profile. Note the origin is located on the landside (Osiberu et al., 2024).

5.2.3 Sand Dune Volumetric Analysis

The sand dune volumetric changes were assessed in MA-4 and MA-6 using both UAV and TS surveys. In MA-4 (Figure 5.9a), UAVs captured an increase in volume from December (4238.48 m^3) to April (5854.64 m^3), while TS surveys also showed a moderate increase in volume throughout the period (5211.63 m^3 in December to 6150 m^3 in April). Also, in MA-6 (Figure 5.9b), UAVs detected a decrease in volume from January (2391.28 m^3) to February (1781.09 m^3), followed by an increase in March (2502.19 m^3), and TS surveys also show the same growth pattern (2010.62 m^3 in December to 3288.67 m^3 in April). Thus, the trend of the volume from both surveying methods at the two locations is similar, which validates the UAV's effectiveness in capturing dynamic changes in coastal dunes.

Although the volume changes from both methods exhibit a similar pattern, there are disparities between the calculated volumes from both methods (Figure 5.9). The relative errors between the two sets of estimated volumes were calculated with a range between 4% (MA-6, December 2022) and 24% (MA-4, March 2023), corresponding to the lowest and highest errors, respectively.
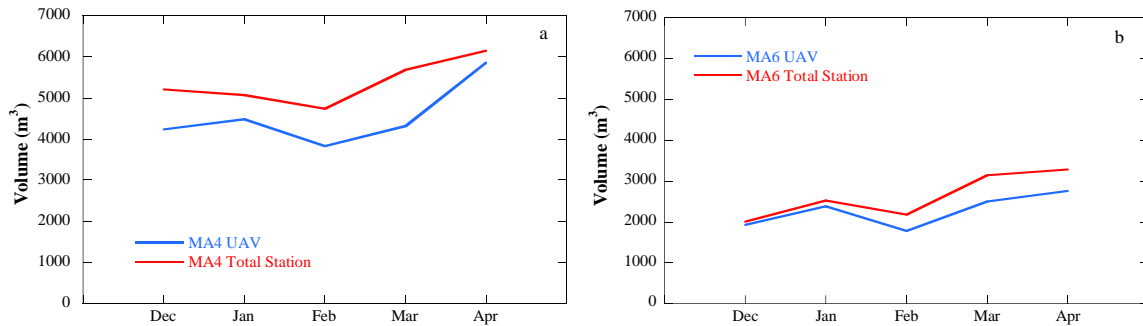

Figure 5.9: Volumetric analysis results, (a) MA-4 and (b) MA-6 (Osiberu et al., 2024).

5.3 Conclusions

      This study provided a comprehensive analysis of survey methods with TS and UAV and their application in monitoring coastal dune restoration at SPI. It advanced our understanding of their practical applications to the monitoring and restoration of coastal dune ecosystems. The results presented offer valuable insights into the effectiveness, accuracy, and adaptability of the survey techniques, contributing to a deeper understanding of coastal dynamics. The creation of DEMs through TS and UAV surveys has been a central focus of this research. These models have provided a detailed and dynamic perspective of coastal topography, allowing for a better understanding of the overall changes in the dune landscape.

Chapter 6. Fiber Mat Reinforcement Material Assessment

Damage to coastal dunes may result in loss of habitat for species, reduced biodiversity, and increased erosion during storms (Bessette et al., 2018) because coastal dunes provide necessary protection for coastline communities (Ajedegba et al., 2019). Plants generally reduce erosion by redirecting incoming water flow above ground and modifying substrate below ground (Sigren et al., 2014). Ongoing research efforts conducted at SPI by TAMUK researchers show that a dune restored with native monocot and coconut fiber mat increases in dune growth and vegetation cover (Patel, 2020). The application of biodegradable coconut fiber in coastal dune restoration has been promoted as a nature-nurturing alternative along the US coast to combat coastal erosion and assist habitat restoration. Coconut fiber, a cost-effective, readily available, sustainable, and biodegradable material can provide additional stability to the coastal dunes and reduce sediment erosion. They can also decrease surface runoff and increase moisture availability in the soil profile (Mapa, 1996, Asha'ari et al., 2021). The coconut-based material biodegrades over time; however, quantitative data on the degradation rate of these fibers in field conditions are very limited. Such information is critical in providing guidance during the design of coastal dune restoration efforts. This chapter reports preliminary results of fiber mat degradation collected in situ from March to June 2024.

6.1 Fiber Mat Installation and New Vegetation Planting

A biodegradable coconut fiber mat was installed on the slope of the dune in MA-4 with the assistance of the Cameron County Parks and Recreation personnel on February 9, 2024. In detail, from January to February 2024, plant recovery was conducted at the plant repository previously established in Isla Blanca Park and sand dune restoration activities were carried out in MA-4 in Isla Blanca Park based on a contract with Cameron County (Contract No.2021C09301).

The plant repository primarily contained Bitta panicum plants, which were recovered from nearby dunes and planted in fall 2021. Due to the recent drought in fall 2023, most plants are in a dry stage, so only 400 plants were recovered between January 3 and 5, 2024. After discussions with Cameron County, over 800 bitter panicum plants were extracted from a nearby location, the north sand dunes pathway. Recovered plants were stored in buckets on January 5 and January 6, 2024.

Due to limited plants recovered, the restoration effort was focused on MA-4. To ensure the sand was suitable for fiber mat installation and drip irrigation, Cameron County provided help in scraping and leveling the sand. The fiber mat installation focused on the foredune, which was determined to be 180 feet wide and 6 feet high (Figure 6.1). A trench 1.5 feet deep was dug at the toe of the foredune to stabilize the fiber mat. Wooden stakes were placed at the top of the fiber mat for additional stability and the coconut fiber mat was installed on February 9, 2024.

The Drip Irrigation system was then installed in coordination with the Cameron County team. The system included a permanent water source channel near the MA-4 walkway and a configured timer set for 6:00 AM and 5:00 PM daily. In the irrigation system, PVC pipes with a diameter of ½ inch were used and connectors and splitters were installed to lay the pipelines above the fiber mat installed beforehand (Figure 6.1). The bottom of the pipelines was perforated to ensure water dripped near the plant stems. The installation of the irrigation system was completed on February 8, 2024, with drip irrigation installation and planting finalized on February 24, 2024.

After the new coconut fiber mats were installed, native vegetation (more than 800 monocot plants) was planted in MA-4 (at the dune toe of the fore dune) on February 9, 2024.

Planting the recovered plants was conducted with the assistance of multiple volunteers including students from the College of Engineering at TAMUK.

Figure 6.1: Installation of fiber mat and drip irrigation on the foredune (February 24, 2024).

6.2 Fiber Mat Degradation Assessment

The first quantitative analysis of the soil core samples after the fiber mat installation was conducted on March 8, 2024. Soil samples were collected to quantify the biodegradable fiber mat at locations Q11, Q12, Q13, and Q14 (Figure 6.2), and the collected soil samples were analyzed following the Standard Test Method. In detail, ASTM D2216 was employed to determine the water (moisture) content, which was conducted by drying 100 g of soil samples at $110°C \pm 5°C$ in an oven for 12 to 16 hours. After oven drying, 50 grams of the soil sample were placed in a furnace and baked at $440 \pm 10°C$ until the degradable materials in the samples were completely turned into ashes (10-15 minutes). The remaining ashes were removed and placed in a desiccator to cool to room temperature before determining their mass. The amount of organic materials, the degradable materials, were then calculated using

$$M_o = M_{cs} - M_a \tag{6.1}$$

where M_o is the degradable materials (g), M_{cs} the sum of the mass of the container and oven-dry soil specimen (g), and M_a the sum of the remaining ashes and the container (g).
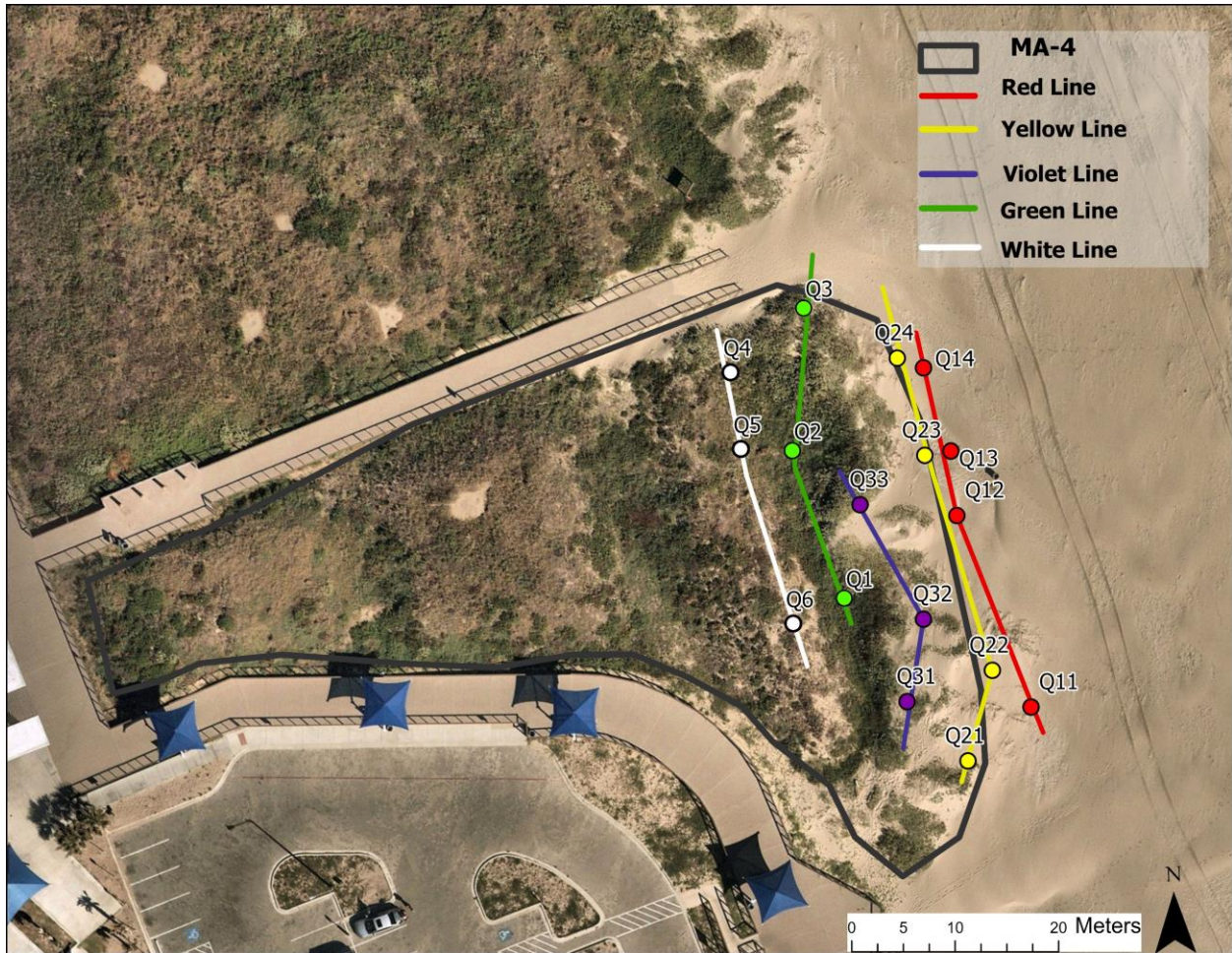
Figure 6.2: Locations of apparent shear strength measurements used at MA-4.

In addition, apparent shear strength was measured using a Geonor H-60 vane tester across the foredune of MA-4 after the new fiber was installed and the vegetation was planted. All apparent shear strength measurements were conducted at depths between 0.75 and 1 ft at locations shown in Figure 6.2. Locations Q11, Q12, Q13, and Q14 (red line) are situated in the area where the new fiber mats were installed. Q21, Q22, Q23, and Q24 (yellow line) are located on the fore dune where no new fiber mats were installed, and no vegetation was planted (all previous vegetation was scraped). Q31, Q32, and Q33 (violet line) are on top of the dune where new vegetation was planted. Q1-Q6 (green and white lines) are the locations used in previous data collection.

71

6.3 Results

Figure 6.3 shows the mass of degradable materials present in the soil samples collected on March 8, May 9, and June 14, 2024. Recall that the fiber mat was installed on Feb. 9, 2024. The first data collected on March 8, 2024 had degradable materials ranging from 6.5 g to 10.9 g per 50 g dry soil sample. The second data set collected on May 9, 2024 had degradable materials ranging from 0.73 to 5.15 g per 50 g dry soil sample. The third data set collected on June 14, 2024 had degradable materials ranging from 0.96 ± 0.17 to 2.02 ± 2.11 g per 50 g dry soil sample. Thus, a significant loss of degradable materials occurred. The calculated degradation rates are 0.0016, 0.0013, 0.0020, and 0.0009 g/g soil/day for locations Q11, Q12, Q13, and Q14, respectively.

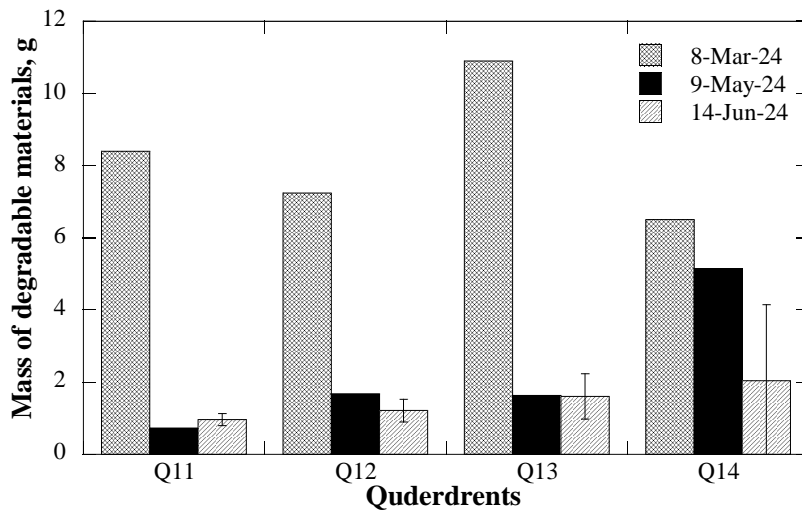Figure 6.3: Mass of degradable material present in 50 grams of soil samples collected. Error bars are standard deviations in three measurements at individual quadrats.

Figure 6.4 shows the shear strength measured on March 8, May 9, and June 14, 2024. At locations where fiber mats were installed (Q11, Q12, Q13, and Q14), the apparent shear strengths were lower than locations at other transect lines. Also, at Q11, Q13, and Q14, the

apparent shear strengths continuously increased from March 8 to June 14. At all other locations except for Q1-Q6, the apparent shear strengths decreased (from March 8 to May 9) and then increased. Recall that no new fiber mats were installed, no vegetation was planted, and previous vegetation was all scarped at Q21, Q22, Q23, and Q24 (yellow line). At Q31, Q32, and Q33 (violet line), only new vegetation was planted, and no fiber mats were installed. This observation indicates that the combined vegetation replanting and fiber mat installation is in favor of soil cohesion growth; however, since only three data sets were collected to date after the new fiber mat installation, it is too early to draw any definite conclusions. More data to be collected at these locations will be needed.
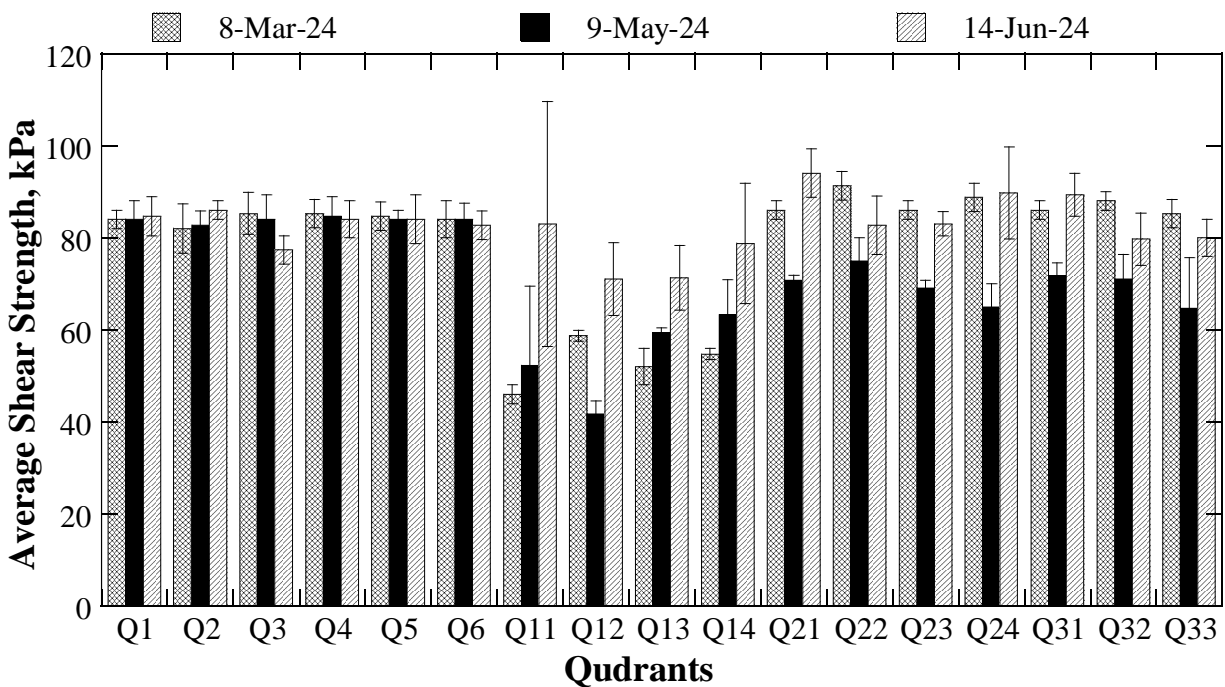

Figure 6.4: Measured shear strength at MA-4.

Figure 6.5 shows the vegetation counted on March 8, May 9, and June 14, 2024. At locations Q11, Q12, Q13, and Q14 (red line) where the new fiber mats were installed, and new monocot vegetation was planted on Feb. 9, 2024, monocot numbers increased then decreased at

Q11, decreased then increased at Q12 and Q13, and decreased at Q14 comparing data collected between March 8 and June 14, 2024. Most of the monocot numbers counted at these locations are higher than those obtained at Q1-Q6, where vegetation has been well established. These observations are promising because Q11, Q12, Q13, and Q14 (red line) are located at the dune toe, where severe erosion often occurs. At Q21, Q22, and Q23, even though no vegetation was planted, some monocots were observed over time. At Q31, Q32, and Q33 (violet line) where new vegetation was planted, monocots increased significantly in May and June 2024, especially at Q32 and Q33. Dicot species also appeared over time at most locations. Note no vegetation removal was conducted at Q31, Q32, and Q33 before planting, so dicots were present naturally at these locations and their growth generally increased over time.
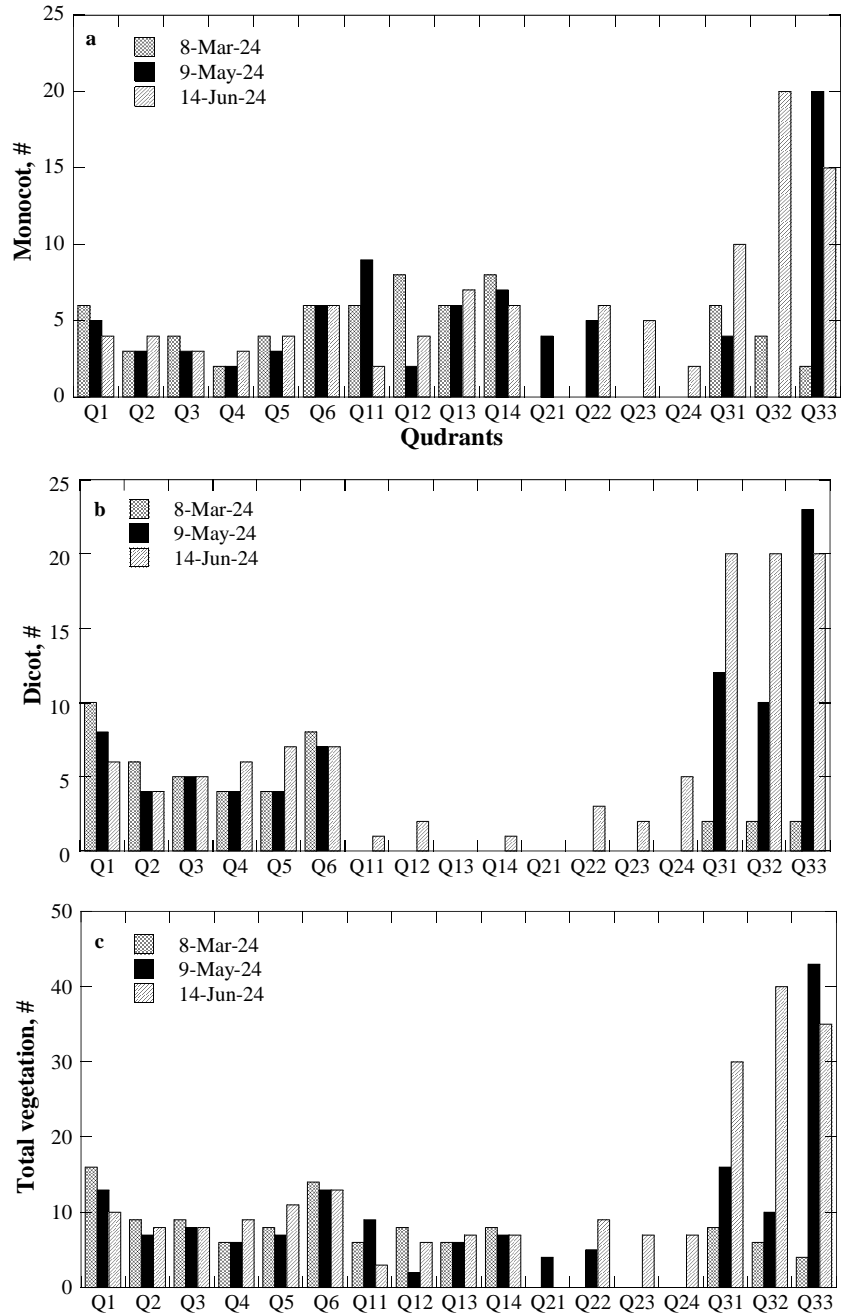
Figure 6.5: Vegetation count in MA-4. a) monocot, b) dicot, and c) total vegetation.

6.4 Conclusions and Discussion

Due to the delay in the installation of the fiber mats, only limited data was collected here.

Based on the limited data collected after fiber mat installation and monocot species replanting, it

was found that fiber mat degraded very fast within the first three months after installation and their degradation rates ranged from 0.0009 to 0.002 g/g soil/day. The fiber mat installed seems to have played a noticeable role in assisting new vegetation establishment and growth. This new vegetation planting and growth in turn might have contributed to an increase in the soil's apparent shear strength. However, to examine further these initial trends/impacts observed, more continued data collection will be needed.

Chapter 7. Recommendation for Future Work

During the project period, extensive data collection and analysis were conducted, and major conclusions were made. The work enhanced our overall understanding of the key underlying issues that are critical in guiding future coastal restoration efforts and the associated data collection for outcome assessment. Some of the key recommendations for future work are summarized below:

1) For future dune restoration projects, planting patterns that prioritize monocot species with long-reaching and fibrous root systems (i.e., maximizing RLD) may help encourage dune growth and the below-ground biomass can further reduce erodibility.

2) We collected extensive vegetation data including vegetation density, root length density (RLD), % vegetation species coverage in this study. However, due to the limitations of field-scale vegetation data collection with respect to spatial and temporal resolutions, the role of vegetation in reinforcing coastal dunes, controlling migrating sand particles, and enhancing dune resilience to storms and tides is still not fully understood. Future studies might consider applying vegetation sensing techniques such as flying UAVs to allow the assessment of large areas with higher temporal resolution and longer periods of monitoring efforts.

3) Further study on the mechanism of the shear strength measurement of vegetated sediment with vane shear should be conducted for a better understanding of the measured shear strength and ultimately to standardize the testing method in field data collection for coastal planning.

4) Although UAVs can be effective in capturing dynamic changes in coastal dunes, even in the face of rapid and dynamic environmental changes, errors can occur depending on the season and weather conditions. Detailed site-specific assessment to quantify the potential errors

caused by these environmental factors on UAV applications will help reduce these expected uncertainties/errors. Particularly, the impact of vegetation on UAV applications needs further investigation.

5) During this project, we used native coastal vegetation collected from local dunes that would otherwise be destroyed due to construction activities in our dune restoration effort. This approach is very time-consuming and labor-intensive. Also, the supply of these plants by this approach is not guaranteed. Future efforts focusing on propagating native vegetation species from plant seeds for dune restoration activities should be pursued.

6) In addition to UAV, other remote sensing data including NDVI should be explored for long-term continuous monitoring of vegetation, coastal dune morphological changes, and social-economic development features in future studies. Such information can help better assess dune resilience to climate challenges.

7) The sand transport model via Bagnold's model showed promise even though differences in dune growth rates were found between those calculated values obtained using Bagnold's model to the ones estimated based on the topographical survey data. Factors such as vegetation, temperature, precipitation, and wave characteristics should be considered in future wind-driven sand transport modeling to better help estimate sediment transport rates. Also, more comparisons between model predictions and field data collected over a longer period will be needed to further evaluate the model performance.

References

AASHTO (2012). Classification of Soils and Soil-Aggregate Mixtures for Highway Construction Purposes. M145-91. Washington DC: American Association of State Highway and Transportation Officials.

Abbate, A., Campbell, J. W., Kimmel, C. B., & Kern, W. H. (2019). Urban development decreases bee abundance and diversity within coastal dune systems. Global Ecology and Conservation, 20, e00711. https://doi.org/10.1016/j.gecco.2019.e00711

Ajedegba, J. O., Choi, J.-W., & Jones, K. D. (2019). Analytical modeling of coastal dune erosion at South Padre Island: A consideration of the effects of vegetation roots and shear strength. Ecological Engineering, 127, 187–194. https://doi.org/10.1016/j.ecoleng.2018.11.020

Ali, F.J. and Normaniza, O.(2008). Shear Strength of a Soil Containing Vegetation Roots, Soils and Foundations, 48(4), 587-596.

American Society for Testing and Materials (ASTM) (2008). ASTM D2573-08. Standard Test Method for Field Vane Shear Test in Cohesive Soil. West Conshohocken, PA, DOI: 10.1520/D2573-08, http://www.astm.org.

American Society for Testing and Materials (ASTM) (2015). ASTMC136-06. Standard Test Method for Sieve Analysis of Fine and Coarse Aggregates. West Conshohocken, PA, DOI: 10.1520/C0136-06, http://www.astm.org.

Andrews, Brian D., Gares, P. A., & Colby, J. D. (2002). Techniques for GIS modeling of coastal dunes. *Geomorphology*, *48*(1–3), 289–308. https://doi.org/10.1016/S0169-555X(02)00186-1

Arens, S. (1997). Transport rates and volume changes in a coastal foredune on a Dutch Wadden island. *Journal of Coastal Conservation*, 49–56.

Asha'ari, M., Rahman, E., Ratnayake, U., Tan, S. J., & Shams, S. (2021). Field evaluation of

using coconut husk and fibre to control slope erosion. *IOP Conference Series: Earth and Environmental Science*, *646*, 012044. https://doi.org/10.1088/1755-1315/646/1/012044

Bagnold, R. (1973). *The Nature of saltation and "bed-load" transport in water*. In Proceedings of the Royal Society of London.

Bagnold, R. (1936). *The movement of desert sand*. Proceedings of the Royal Society of London.

Bagnold, R.A. (1941). *The Physics of Blown Sand and Desert Dunes*. 265 pages. London: Methuen.

Barba, S., Barbarella, M., Di Benedetto, A., Fiani, M., Gujski, L., & Limongiello, M. (2019). Accuracy Assessment of 3D Photogrammetric Models from an Unmanned Aerial Vehicle. Drones, 3(4), 79. https://doi.org/10.3390/drones3040079

Barros, P. L. A. and Barros, C. L. A. (1989). Vane shear test application on cohesionless soils, Proceedings of 12th International Conference on Soil Mechanics and Foundation Engineering, Rio de Janeiro, 13–18 August, 1989, 171 – 174.

Bessette, S. R., Hicks, D. W., & Fierro-Cabo, A. (2018). Biological assessment of dune restoration in south Texas. Ocean and Coastal Management, 163, 466-477. doi:10.1016/j.ocecoaman.2018.06.019

Bonte, D., Lens, L., & Maelfait, J. (2006). Sand dynamics in coastal dune landscapes constrain diversity and life-history characteristics of spiders. Journal of Applied Ecology, 43(4), 735–747. https://doi.org/10.1111/j.1365-2664.2006.01175.x

Bryant, D. B., Anderson Bryant, M., Sharp, J. A., Bell, G. L., & Moore, C. (2019). The response of vegetated dunes to wave attack. Coastal Engineering, 152, 103506. doi:10.1016/j.coastaleng.2019.103506

Ciavola, P., Ferreira, O., Dongeren, A. V., Vries, J. V. T. de, Armaroli, C., & Harley, M. (2014). Prediction of Storm Impacts on Beach and Dune Systems. In P. Quevauviller (Ed.), Hydrometeorological Hazards (pp. 227–252). John Wiley & Sons, Ltd. https://doi.org/10.1002/9781118629567.ch3d

City of New York (2013). PlanNYC: a Stronger, More Resilient New York. The City of New York, New York, NY. http://www.nyc.gov/html/sirr/html/report/report.shtml.

Del Angel, D. (2011). *Dune-beach morphodynamic interaction along a semi-arid, wave dominated barrier island: South Padre Island, Texas*. Texas A&M University - Corpus Christi.

Dong, Z., Liu, X., Wang, H., & Wang, X. (2003). Aeolian sand transport: A wind tunnel model. *Sedimentary Geology*, 71–83.

Durán Vinent, O. Schaffer, B. E., and Rodriguez-Iturbe, I. (2020) Stochastic dynamics of barrier island elevation 118 (1), e2013349118.

Environmental Protection Agency (EPA) (2023) Climate Change Impacts on Coasts, https://www.epa.gov/climateimpacts/climate-change-impacts-coasts#:~:text=3.-,Land%20Losses,especially%20on%20the%20Gulf%20Coast.&text=Rising%20sea%20levels%20can%20turn,can%20also%20be%20at%20risk.

Fan, C.-C. and Su, C.-F. (2008). Role of roots in the shear strength of root-reinforced soils with high moisture content, Ecological Engineering, 33(2), 157-166.

Farrent, T. A. (1960). "The interpretation of vane tests in soils having friction." Proceedings of 3rd Australia-New Zealand Conference on Soil Mechanics and Foundation Engineering, 81-88.

Fattet, M., Fu, Y., Ghestem, M., Ma, W., Foulonneau, M., Nespoulous, J., . . . Stokes, A. (2010).

    Effects of vegetation type on soil resistance to erosion: Relationship between aggregate

    stability and shear strength. Catena, 87, 60-69. doi:10.1016/j.catena.2011.05.006

Feagin, R., Rusty, A., Figlus, J., Zinnert, J. C., Sigren, J., Martínez, M. L., . . . Carter, G. (2015).

    Going with the flow or against the grain? The promise of vegetation for protecting

    beaches, dunes, and barrier islands from erosio. Frontiers in Ecology and the

    Environment, 13(4), 203-210. doi:10.1890/140218

Gallego-Fernández, J. B., Sánchez, I. A., & Ley, C. (2011). Restoration of isolated and small

    coastal sand dunes on the rocky coast of northern Spain. Ecological Engineering, 37(11),

    1822–1832. https://doi.org/10.1016/j.ecoleng.2011.06.017

Gray, D.H. and Leiser, A.T. (1982). Biotechnical Slope Protection and Erosion Control. Van

    Nostrand Reinhold Company. New York

Griggs, G., & Reguero, B. G. (2021). Coastal Adaptation to Climate Change and Sea-Level Rise.

    Water, 13(16), Article 16. https://doi.org/10.3390/w13162151

Hamzah, M. B. A.-H., & Omar, S. B. A.-A. (2018). A review on the angle of repose of granular

    materials. *Powder Technology*, *330*, 397–417.

Houser, C., & Mathew, S. (2011). Alongshore variation in foredune height in response to

    transport potential and sediment supply: South Padre Island, Texas. Geomorphology, 125(1),

    62–72. https://doi.org/10.1016/j.geomorph.2010.07.028

Hsu, S.A. (1977). Boundary - layer meteorological research in the coastal zone, Geoscience and

    Man, 18, 99-111

Intergovernmental Panel on Climate Change (IPCC) (2021a) Climate Change 2021: The

    Physical Science Basis. Contribution of Working Group I to the Sixth Assessment Report of

the Intergovernmental Panel on Climate Change, Cambridge University Press, Cambridge, United Kingdom and New York, NY, USA,

Intergovernmental Panel on Climate Change (IPCC). (2021b). Ch. 11: Weather and climate extreme events in a changing climate. In: Climate change 2021: The physical science basis. Contribution of Working Group 1 to the Sixth Assessment Report of the IPCC. Cambridge University Press. In press, p. 11-6.

Jin, D., Hoagland, P., Au, D. K., & Qiu, J. (2015). Shoreline change, seawalls, and coastal property values. Ocean & Coastal Management, 114, 185–193. https://doi.org/10.1016/j.ocecoaman.2015.06.025

Judd, F.W, Lonard, R.I. and Sides. S.L. (1977). The Vegetation of South Padre Island, Texas in relation to Topography, The Southwestern Naturalist, 22(1), 31–48, https://doi.org/10.2307/3670462.

Judd, F.W., Summy, K.R., Lonard, R.I., Mazariegos, R. (2008). Dune and Vegetation Stability at South Padre Island, Texas, United States of America, Journal of Coastal Research, 24(4), 992-998.

Judd, F.W., and Sides, S.L. (1983). The Effect of Hurricane Allen on the Near-Shore Vegetation of South Padre Island, The Southwestern Naturalist, 28(3), 365–69, https://doi.org/10.2307/3670799.

Khalil, R. (2013). The Accuracy of GIS Tools for Transforming Assumed Total Station Surveys to Real World Coordinates. Journal of Geographic Information System, 05(05), 486–491. https://doi.org/10.4236/jgis.2013.55045

Lancaster, N., & Baas, A. (1998). Influence of vegetation cover on sand transport by wind: Field

    studies at Owens Lake, California. Earth Surface Processes and Landforms, 23, 69–82.

    https://doi.org/10.1002/(SICI)1096-9837(199801)23:13.0.CO;2-G

Lee, J.-M., Park, J.-Y., & Choi, J.-Y. (2013). Evaluation of Sub-aerial Topographic Surveying

    Techniques Using Total Station and RTK-GPS for Applications in Macrotidal Sand Beach

    Environment. Journal of Coastal Research, 65, 535–540. https://doi.org/10.2112/SI65-091.1

Lettau K, Lettau H.H. (1978). Experimental and micrometeorological field studies of dune

    migration. In Exploring the World's Driest Climate, Lettau HH, Lettau K (eds). University of

    Wisconsin-Madison: Madison, WI; 110–147.

Lonard, R.I., Judd, F.W., Everitt, J.H., Escobar, D.E., Alaniz, M.A., Cavazos, I., and Davis, M.R.

    (1999). Vegetative Change on South Padre Island, Texas, over Twenty Years and Evaluation

    of Multispectral Videography in Determining Vegetative Cover and Species Identity, The

    Southwestern Naturalist, 44(3), 261–71. http://www.jstor.org/stable/30055221.

Martínez, M. L., Gallego-Fernández, J. B., García-Franco, J. G., Moctezuma, C., & Jiménez, C.

    D. (2006). Assessment of coastal dune vulnerability to natural and anthropogenic

    disturbances along the Gulf of Mexico. Environmental Conservation, 33(2), 109–117.

    https://doi.org/10.1017/S0376892906002876

MacDonald, K. A., B. A. Coutermarsh, S. A. Shoop, and W. T. Burch, (2012). A New Method to

    Measure Vegetated Soil Shear Strength Using the Vegetation and Soil Shear Tester

    (VASST). In Proceedings of the 12th European Conference of the International Society for

    Terrain-Vehicle Systems (ISTVS), 24–27 September, Pretoria, South Africa.

Mapa, R. (1996). Coconut fiber: A bio-degradable soil erosion control. *Biological Agriculture*

    and Horticulture, *13*, 149–160.

Miller, R. and Jastrow, J. (1990). Hierarchy of Root and Mycorrhizal Fungal Interactions with

    Soil Aggregation, Soil Biology and Biochemistry, 22, 579-584.

National Park Service. (2022). Geologic Formations. Retrieved from NPS.gov:

    https://www.nps.gov/pais/learn/nature/geologicformations.htm

Nesbit, P. R., Hubbard, S. M., & Hugenholtz, C. H. (2022). Direct Georeferencing UAV-SfM in

    High-Relief Topography: Accuracy Assessment and Alternative Ground Control Strategies

    along Steep Inaccessible Rock Slopes. Remote Sensing, 14(3), 490.

    https://doi.org/10.3390/rs14030490

NOAA National Center for Environmental Information. (2022). Climate at a Glance: City Time

    Series. Retrieved from https://www.ncei.noaa.gov/cag/.

Nordstorm, K. F., & Jackson, N. L. (2022). *Beach and Dune Restoration* (Second). Cambridge

    University Press.

NOAA Tides and Currents (2020). https://tidesandcurrents.noaa.gov/

Osiberu, O.A., J-W., Choi and J. Ren (2024). Effects of Vegetation and Wind on Assessing

    Spatial and Temporal Coastal Dune Changes using UAV and Total Station Surveys, *Journal

    of Coastal Research*, in review.

Osman, N. and S.S. Barakbah, (2006), Parameters to predict slope stability - Soil water and root

    profiles, Ecological Engineering, 28(1), 90-95.

Park, Sung-Sik, Zhou, An, and Kim, Dong-Rak. (2016). Vane Shear Test on Nakdong River

    Sand. KSCE Journal of Civil and Environmental Engineering Research, 36(3), 463–470.

    https://doi.org/10.12652/KSCE.2016.36.3.0463; (in Korean).

Patel, K. (2020). Evaluation of the effects of native vegetation cover and root density on coastal

    dunes- an approach to reduce coastal erosion at South Padre Island, Texas, USA. Texas

    A&M University- Kingsville, Environmental Engineering (Unpublished).

Pollen, N. (2007). Temporal and spatial variability in root reinforcement of streambanks:

    Accounting for soil shear strength and moisture, CATENA, 69(3), 197-205.

Pollen, N., and Simon, A. (2005). Estimating the mechanical effects of riparian vegetation on

    stream bank stability using a fiber bundle model, Water Resources Research, 41, W07025.

Reubens, B., Poesen, J., Danjon, F. et al. (2007). The role of fine and coarse roots in shallow

    slope stability and soil erosion control with a focus on root system architecture: a review.

    Trees, 21, 385–402

Sherman, S., Jackson, D., Namikas, S., & Wang, J. (1998). Wind-blown sand on beaches: An

    evaluation of models. *Geomorphology*, *22*, 113–133.

Sigren, J., Figlus, J., and Armitage, A. R. (2014). Coastal sand dunes and dune vegetation:

    Restoration, erosion, and storm protection. Shore and Beach, 82, 5-12.

Silva, R., Martínez, M., Odériz, I., Mendoza, E., & Feagin, R. (2016). Response of vegetated

    dune–beach systems to storm conditions. Coastal Engineering, 109, 53-62.

    doi:10.1016/j.coastaleng.2015.12.007

Simon, A. and Collison, A.J.C. (2002). Quantifying the mechanical and hydrologic effects of

    riparian vegetation on streambank stability, Earth Surface Processes And Landforms, 27(5),

    527-546

Snavely, N., Seitz, S. M., & Szeliski, R. (2008). Modeling the World from Internet Photo

    Collections. International Journal of Computer Vision, 80(2), 189–210.

    https://doi.org/10.1007/s11263-007-0107-3

Taddia, Y., Corbau, C., Zambello, E., & Pellegrinelli, A. (2019). UAVs for Structure-From-
Motion Coastal Monitoring: A Case Study to Assess the Evolution of Embryo Dunes over a
Two-Year Time Frame in the Po River Delta, Italy. Sensors, 19(7), 1717.
https://doi.org/10.3390/s19071717

Termini, D., and Fichera, A. (2020). Experimental Analysis of Velocity Distribution in a Coarse-
Grained Debris Flow: A Modified Bagnold's Equation. *Water*, *12*, 1–19.

U.S. Army Corps of Engineers (USACE) (2013). Hurricane Sandy Coastal Projects Performance
Evaluation Study, Disaster Relief Appropriations Act, 2013. Submitted by the Assistant
Secretary of the Army for Civil Works, November 6, 2013.

USACE. (1984). Shore Protection Manual—Volume I (Vol. 1). United States. Army. Corps of
Engineers, Coastal Engineering Research Center (U.S.), Dept. of the Army, Waterways
Experiment Station, Corps of Engineers, Coastal Engineering Research Center, Vicksburg,
MS. 1984, RN 735-17c.

van der Wal, D. (1996). The development of a digital terrain model for the geomorphological
engineering of the 'rolling' foredune of Terschelling, the Netherlands. Journal of Coastal
Conservation, 2(1), 55–62. https://doi.org/10.1007/BF02743037

Veylon G, Ghestem M, Stokes A, Bernard A. 2015 Quantification of mechanical and hydric
components of soil reinforcement by plant roots, Canadian Geotechal Journal, 52, 1839–1849

Waldron, L. (1977). The Shear Resistance of Root-Permeated Homogeneous and Stratified Soil.
Soil Science Society America Journal, 41, 843-849.
doi:10.2136/sssaj1977.03615995004100050005x

Waldron, L. J. and Dakessian, S. (1981). Soil reinforcement by roots calculation of increased soil
shear resistance from root properties, Soil Science 132(6), 427-435.

Walling, K., Miller, J.K., Herrington, T.O., Eble, A. (2014). Comparison of Hurricane Sandy

impacts in three New Jersey coastal communities. In: Proceedings of the 34th Conference on

Coastal Engineering, Seoul, Korea).

Wieder, W. L., and Shoop, S. A. (2018). State of the knowledge of vegetation impact on soil

strength and trafficability. Journal of Terramechanics, 78, 1-14.

doi:10.1016/j.jterra.2018.03.006

Wieder, W.L. and Shoop, S.A. (2017). "Vegetation impact on soil strength: A state of the

knowledge review", ERDC/CRREL SR-17-2, https://apps.dtic.mil/sti/pdfs/AD1036307.pdf.

Wu, T. H. and Watson, A. (1998). In situ shear tests of soil blocks with roots, Canadian

Geotechnical Journal, 35(4), 579-590.

Wu, T. H., Beal, P. E., & Chinchun, L. (1988). In-Situ Shear Test of Soil-Root Systems. Journal

of Geotechnical Engineering, 112(12), 1376-1394. doi:10.1061/(ASCE)0733-

9410(1988)114:12(1376)

Wyoming Department of Transportation, (2014). Survey Manual: Retrieved from

dot.state.wy.us/home/engineering_technical_programs/photos_and_surveys/SurveyManual.ht

ml.

Yildiz, A., Graf, F., Rickli, C., and Springman, S.M. (2018). Determination of the shearing

behaviour of root-permeated soils with a large-scale direct shear apparatus, CATENA, 166,

98-113.

Zaghloul, N. A. (1992). A computer model to calculate potential eolian sand drift rates.

Advances in Engineering Software, 14(3), 195–204. https://doi.org/10.1016/0965-

9978(92)90022-8

Zimmerman, T., Jansen, K., & Miller, J. (2020). Analysis of UAS Flight Altitude and Ground

    Control Point Parameters on DEM Accuracy along a Complex, Developed Coastline. Remote

    Sensing, 12(14), 2305. https://doi.org/10.3390/rs12142305

Zhang, C.-B., Chen, L.-H., Jiang, J. (2014). Why fine tree roots are stronger than thicker roots:

    The role of cellulose and lignin in relation to slope stability, Geomorphology, 206, 196-202.

Zingg, A. (1952). *Wind tunnel studies of the movement of sedimentary material* (pp. 111–135).

    Proceedings of the 5th Hydraulic Conference Bulletin.